Tang *et al. Biochar* (2025) 7:122
https://doi.org/10.1007/s42773-025-00554-z

Biochar

ORIGINAL RESEARCH Open Access

Biochar: from agricultural waste byproducts to novel adsorbents for ammonia and micro/nanoplastics (MNPs)

Ruogu Tang[1], Siyu Qiu[1], Changqing Wu[1] and Juzhong Tan[1*]

Abstract

Biochar, a stable carbon material derived from biomass pyrolysis, shows promise in agriculture and environmental remediation due to its high porosity, surface area, and ion exchange capacity. Its effectiveness as a filter for emerging contaminants like ammonia and micro/nanoplastics (MNPs) depends on feedstock type and pyrolysis conditions. This study first evaluated biochars produced from corn cob, cocoa husk, walnut shell, and bamboo under varying pyrolysis temperatures and residence times. Comprehensive characterization included elemental composition, porosity, surface functional groups, and polycyclic aromatic hydrocarbons (PAHs). Woody feedstocks (bamboo, walnut) yielded biochars with higher carbon content, surface area, and pore volume, while corn cob biochars provided balanced properties that warranted detailed investigation. Increasing pyrolysis temperature and time enhanced these properties but reduced oxygen-containing functional groups and variably affected PAH levels. Subsequent adsorption studies focused on corn cob biochars. Filtration tests with ammonia (1–100 ppm) and polystyrene MNPs (0.10–2.10 µm, up to 2×10^7 particles/mL) showed that high-temperature samples achieved the best performance. Corn cob biochar prepared at 700 °C for 2.5 h removed 63.95% of ammonia (10 ppm, 30 g loading) and 97.99% of MNPs, with removal efficiency influenced by pyrolysis conditions, biochar load, and contaminant concentration. Importantly, no detectable release of 16 EPA priority PAHs was observed in leaching tests, confirming environmental safety. Regeneration experiments further demonstrated that corn cob biochars could be re-pyrolyzed and reused for three cycles with only modest efficiency losses, with CCB700 maintaining > 55% ammonia removal after Cycle 3. These findings highlight biochar's potential as a sustainable, low-cost, and reusable filtration material for water treatment. Produced from agricultural residues, biochar can mitigate emerging contaminants when engineered under optimized pyrolysis conditions while minimizing environmental risks, supporting its practical application in eco-friendly wastewater treatment systems.

Highlights

- Biochars derived from agricultural byproducts effectively removed >90% of microplastics and up to 64% of ammonia from contaminated water.
- Feedstock type and pyrolysis conditions significantly influenced the porosity, surface area, and adsorption performance of biochar.
- Optimized biochars offer a low-cost, sustainable solution for the removal of ammonia and micro/nanoplastics in water treatment.

*Correspondence:
Juzhong Tan
jztan@udel.edu
[1]Department of Animal and Food Sciences, College of Agriculture and Natural Resources, University of Delaware, Newark, DE 19713, USA.

Springer

Keywords Water treatment, Biochar, Pyrolysis, Ammonia, Micro/nanoplastic, Contaminant adsorption

Graphical Abstract

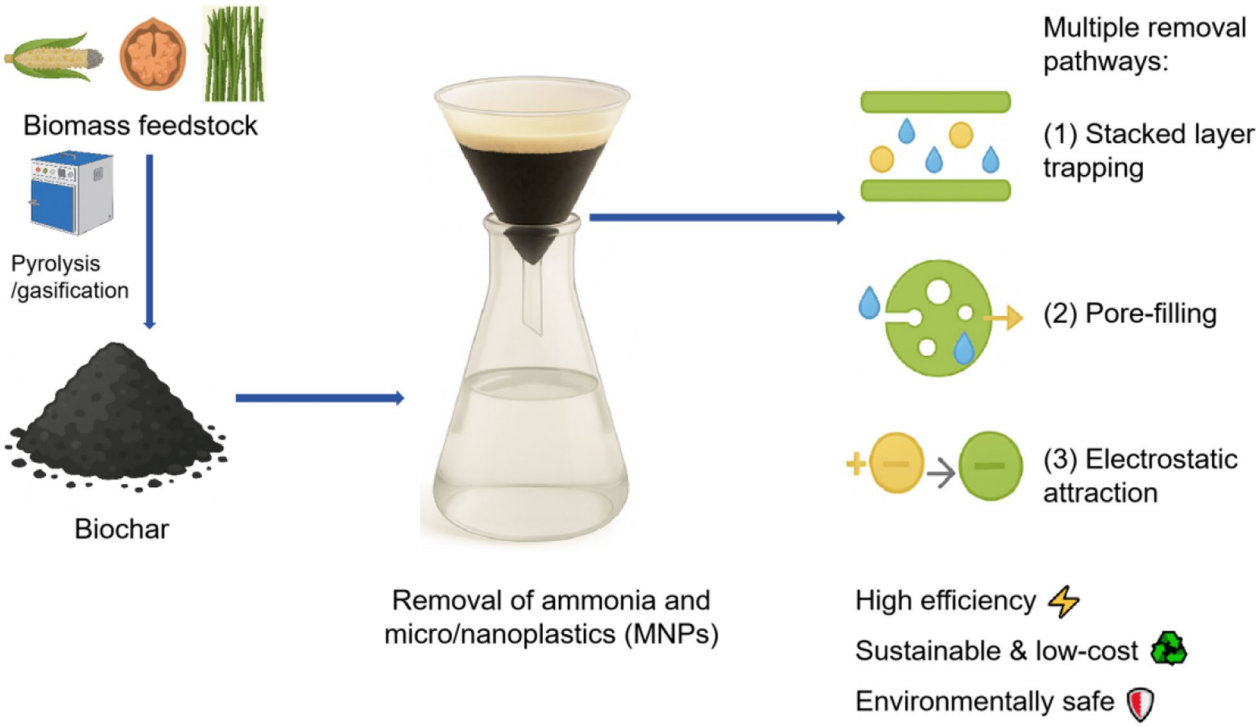

1 Introduction

Wastewater pollution is a critical global issue, with urbanization, agriculture, and industrial activities generating ~ 380 trillion liters of contaminated water annually (Cosgove And Loucks 2015). These waters often contain harmful pollutants such as ammonia, pesticides, PFAS, and micro/nanoplastics (MNPs), leading to serious environmental and health risks (Chen 2024). Untreated discharges contribute to pollution, biodiversity loss, eutrophication, and public health crises (Babuji et al. 2023; Lyiola et al. 2022). Water contamination also impacts agriculture and industry by reducing water availability, degrading land, and increasing maintenance and treatment costs (Weerasooriya et al. 2021).

Among the water contaminants, ammonia and MNPs are of particular concern due to their severe environmental and human health impacts. Ammonia is toxic to aquatic organisms even at low levels; concentrations above 0.5 mg/L NH_3–N can inhibit fish growth, and levels of 2 mg/L can be lethal to sensitive species such as salmonids (Boyce 2023). For humans, chronic exposure through drinking water has been linked to neurological and reproductive disorders (Zhu et al. 2021). Ammonia contamination is widespread, originating from livestock effluents, fertilizer runoff, and industrial discharges, and it remains a key contributor to eutrophication in rivers and lakes (Farghali et al. 2024). On the other hand, ammonia is also a vital nitrogen source for fertilizers and a raw material for plastics, textiles, and dyes, highlighting the dual challenge of mitigating its ecological risks while enabling resource recovery (Mousavi et al. 2022). Given its dual nature as both a pollutant and a valuable material, the removal and recycling of ammonia from contaminated water are critical for safeguarding ecosystem health while supporting economic sustainability.

Micro- and nanoplastics (MNPs) have emerged as a persistent and less tractable contaminant (Li et al. 2024). Recent surveys report microplastic concentrations exceeding 10^6 particles/m^3 in rivers near wastewater treatment plants, and their ingestion has been documented in more than 100 aquatic species, including commercially important fish and shellfish (Sharma et al. 2024). Laboratory studies show that ingested MNPs can induce oxidative stress, disrupt endocrine function, and

impair growth in fish and invertebrates (Haque et al. 2024). For humans, MNPs have been detected in drinking water, salt, and even placental tissue, raising concerns about long-term health effects (Crini And Lichtfouse 2019) Unlike conventional pollutants, MNPs are not effectively removed by standard wastewater treatment processes, facilitating their accumulation and potential biomagnification in food chains (Dey And Uddin 2021).

Addressing both ammonia and microplastics in contaminated water treatment is crucial for mitigating environmental risks and ensuring water quality. However, despite advances in wastewater treatment technologies, several technical bottlenecks remain unresolved. Conventional adsorbents and filtration materials such as activated carbon, ceramic filters, and activated alumina are effective for certain pollutants (e.g., heavy metals, fluoride, and ammonium), but their performance against emerging contaminants such as micro/nanoplastics (MNPs) remains limited (Crini And Lichtfouse 2019). Additionally, their application is further constrained by high operational costs when treating large water volumes, difficulties in regeneration, and the risk of secondary pollution from spent adsorbents or plastic-based filtration media (Kesari et al. 2021). Moreover, most current studies focus on single contaminant classes in isolation, leaving the simultaneous removal of chemically distinct pollutants—ionic species like ammonia and particulate contaminants like MNPs—largely unexplored (Arbabi et al. 2023). These gaps highlight the dual challenges and urgent need for multifunctional, cost-effective, and environmentally safe adsorbents capable of addressing both traditional and emerging contaminants under practical treatment conditions.

To address this gap, the present study investigates biochar as a sustainable and multifunctional filtration material for the simultaneous removal of ammonia and micro/nanoplastics from water. Biochar is a stable form of carbon that is produced from a variety of biomass, namely, agricultural waste byproducts (Patra et al. 2021). It is considered a sustainable and environmentally friendly material that has been gaining increasing attention for its capability to reduce carbon footprints and potential applications in many sectors, including water filtration and contaminant removal (Fawzy et al. 2021; Chen et al. 2019). Compared with other carbon-rich materials, biochar possesses many unique physicochemical and structural properties. Biochar typically has a high fixed carbon content due to the stabilization of carbon through pyrolysis, making it an effective and stable carbon sink. Additionally, its high surface area and porous structure enhance its ability to retain water and essential nutrients. Furthermore, the properties of biochar vary depending on the biomass feedstock and pyrolysis conditions, resulting in different oxygen-containing functional groups (OCFGs) (Fan et al. 2018). These OCFGs, including hydroxyl (-OH), carboxyl (-COOH), carbonyl groups (-C=O) and phenolic groups (aromatic-OH), have been widely recognized as key active sites for ion exchange, metal chelation, and nutrient retention (Zhou et al. 2022; Liu et al. 2023). Prior studies also reported that pyrolysis conditions strongly influence pore development and surface chemistry, which in turn regulate adsorption performance (Luo et al. 2023).

With these features, biochar has been investigated and is recognized as an effective medium for capturing and immobilizing various contaminants from water sources, including heavy and toxic metal ions, inorganic nutrients, such as ammonium, nitrate, and phosphate, and organic nutrients (Luo et al. 2023; Patel et al. 2022). Multiple biochar-contaminant adsorption mechanisms were proposed and validated, including ion exchange, surface complexation, electrostatic attraction, and porous physical adsorption, contingent on the specific ions and environmental conditions. Many previous studies demonstrated that biochar exhibits varying levels of effectiveness in adsorbing toxic and heavy metal ions, such as lead, cadmium, chromium, zinc, and nickel (Chen et al. 2023; Gao et al. 2023). For example, date seed-based biochar showed remarkable adsorption capacity for lead ions through surface complexation effects (Mahdi et al. 2018), while chicken manure-based, oat hull-based, and pine bark-based biochars achieved strong Cu^{2+} and Zn^{2+} adsorption through electrostatic attractions (Zahra et al. 2022). Also, a recent study showed that rice husk biochars can exhibit different adsorption mechanisms under different conditions (Bushra And Remya 2024a). The adsorption was primarily attributed to pore-filling, but when pH was below 5, the surface complexation became prominent, and in concentrated lead or zinc environments, the ion exchange became a major effect (Bushra And Remya 2024a). The hybrid adsorption pathways are also applied in the adsorption of inorganic and organic nutrients by biochar. One previous study showed the mechanisms of adsorbing ammonium by biochar, which indicated that although ion exchange was the predominant contributor, the surface complexation also facilitated the adsorption process, especially at higher temperatures (Xu et al. 2022). Similarly, this phenomenon was also reported in the adsorption of phosphate, as the acting adsorption mechanisms were found to be dependent on pH, temperature, and phosphate species (Luo et al. 2023). More recently, Zhao et al. demonstrated that coupling biodegradable microplastics with biochar can enhance cadmium chelation and reduce plant Cd uptake, highlighting how biochar can simultaneously interact with emerging contaminants and heavy metals

in complex environmental systems (Zhao et al. 2025). In addition to ionic species, biochar has also been explored for removing MNPs from water. Current studies suggest that retention is primarily achieved through structural pathways such as surface trapping and pore-filling, with electrostatic attraction playing an additional role under certain pH conditions (Subair et al. 2024; Ahmed et al. 2016). However, research on biochar–MNP interactions remains limited, and further efforts are needed to clarify mechanisms and optimize performance against particulate contaminants. In this context, recent studies have increasingly focused on the modifications of biochar, including surface treatment and functionalization, grafting and coating with new moieties, and hybrid additives or biological activation, which can effectively enhance adsorption capacities (Kumar et al. 2022).

Despite its potential as an adsorbent and filtration material, biochar faces several challenges that hinder its widespread application. Its physicochemical, structural, and techno-functional properties vary significantly depending on pyrolysis conditions and feedstock, yet there is a knowledge gap in optimizing these conditions to achieve desirable properties cost-effectively (Gai et al. 2014). Before biochar-based water filters can be widely adopted and scaled up, their configurations and filtration conditions require comprehensive investigations. Additionally, current research has primarily focused on conventional contaminants, while the adsorption mechanisms for emerging contaminants are still not well understood (Siipola et al. 2020). Another critical challenge is the potential secondary contamination from biochar itself. Depending on the pyrolysis conditions and the feedstock, biochar contains varied levels of polycyclic aromatic hydrocarbons (PAHs), which may leach into the water and pose a risk of secondary contamination (Buss et al. 2022). To address these concerns, significant research work needs to be done to investigate the impacts of pyrolysis and the type of feedstock on the characteristics of biochar as filtration materials and the cost-effectiveness of the filtration practices.

This study explored the use of biochar made from a variety of agricultural wastes as adsorbents for removing contaminants from water. Biochar was produced from agricultural biomass through pyrolysis under varying conditions. The resulting biochars were characterized in terms of morphology, composition, and surface properties, while the effects of pyrolysis conditions on biochar production were also examined. For wastewater treatment, the optimal biochars were ground into fine powders suitable for filtration. A model filtration system was used to treat water samples containing either ammonia or polystyrene micro/nanoplastics (PS-MNPs) at different concentrations. The adsorption efficiency was evaluated separately for each contaminant, and the corresponding adsorption mechanisms were subsequently investigated respectively. This study therefore aimed to compare biochar's performance against a dissolved nutrient (ammonia) and an emerging particulate contaminant (PS-MNPs), in order to elucidate how biochar properties influence adsorption pathways across distinct pollutant classes. In addition, practical application of biochar filters depends not only on initial adsorption but also on their potential for reuse. To address this, a preliminary regeneration test was performed in which biochars used for 10 ppm ammonia removal were re-pyrolyzed and re-tested, allowing comparison of adsorption efficiency across cycles.

2 Methods

2.1 Biochar preparations

In this study, biochars were obtained by pyrolysis or gasification of agricultural waste byproducts, including corn cobs, cocoa husks, nutshells, bamboo, and poultry litter (Table 1). Poultry litter biochars were produced by gasification at 1000 °C for 2.5 h under atmospheric pressure in an oxygen-limited reactor (Joardar et al. 2020). Corn, cocoa husk, nutshell, and bamboo biochars were produced by pyrolysis of the corresponding feedstocks (sourced from local farms): corn cob stalks, peeled cocoa husks, matured nutshells, and bamboo stalks (Amin

Table 1 Preparations of biochars from various feedstocks

Biochar type	Feedstock	Producing method	Temperature	Residence time
Corn cob biochars (CCB)	Peeled corn cob stalks	Pyrolysis	350, 550, or 700 °C	1.5 h or 2.5 h
Cocoa husk biochar (CHB)	Peeled cocoa husks	Pyrolysis	350, 550, or 700 °C	1.5 h or 2.5 h
Walnut shell biochar (WSB)	Matured nutshell	Pyrolysis	350, 550, or 700 °C	1.5 h or 2.5 h
Bamboo stalk biochar (BSB)	Bamboo stalks	Pyrolysis	350, 550, or 700 °C	1.5 h or 2.5 h
Poultry litter biochar (PLB)	Poultry litters	Gasification	1000 °C	2.5 h

2018; Tsai et al. 2018; Dias et al. 2025; Kumar et al. 2025). Prior to pyrolysis, corn cobs and bamboo stalks were peeled to remove straws and leaves, then cut into ~ 10 cm pieces.

In the pyrolysis process, the biomass was individually kept in a stainless steel crucible and placed into a muffle furnace (Model QCF-1200, Across International LLC, Livingston, NJ, USA). The pyrolysis was carried out under −15 psi, and the pyrolysis temperatures were set at 350 °C, 550 °C, or 700 °C. The heating rate of the pyrolysis processes was 20 °C/min and the residence time was 1.5 or 2.5 h. Upon the completion of the pyrolysis process, the furnace was shut down, and the samples were left in the furnace chamber until the furnace was cooled down to room temperature (within 1 h). The yields of the resulting biochar samples were calculated as in Eq. 1:

$$Yields\% = \frac{Massofbiochar/g}{Massofcornstock/g} \times 100 \quad (1)$$

2.2 Biochar characterizations

The resulting biochar samples were milled and ground into particles by hammers with an average particle size of 779.76 μm. This particle size was chosen to balance handling convenience with structural integrity, while also ensuring consistent loading in the funnel filtration system. The microstructure and morphologies of the biochar samples were observed via the scanning electron microscope (SEM, Apreo 2 VolumeScope™, Thermo Fisher Scientific Inc., Waltham, MA, USA) with platinum sputtering. The compositions of biochars, including total carbon, hydrogen, and oxygen contents, were measured via elemental analysis (Vario EL cube Elementar Analyzer 6720, Elementar Inc., Ronkonkoma, NY, USA). About 10 mg of biochar samples were combusted for 120 s and analyzed, and the H/C and O/C molar ratios were then calculated. The mineral contents (P, K, Ca, Mg, Zn, Fe, etc.), pH and cation exchange capacity (CEC) were analyzed by the Mehlich 3 extraction-based analysis routine. The polycyclic aromatic hydrocarbons contents were investigated by a GC–MS system (Intuvo GC-MSD/Agilent 7697A, Agilent, Santa Clara, CA, USA), 10 μg of biochar was suspended in 100 μL dichloromethane for the test, and the contents of PAHs were calculated by integrating and comparing with NIST Research Library (Buss et al. 2022). The surface area, pore size, and volume were measured and investigated by the Brunauer–Emmett–Teller (BET) method (Micromeritics ASAP 2020 BET Analyzer, Micromeritics Instrument Corporation, Norcross, GA, USA), approximately 150 mg of biochar samples were used with thermal isolation protection. Zeta potential measurements were performed on Wyatt Mobius DLS Zeta (Wyatt Technology LLC, Santa Barbara, CA), prior to the test, 0.1 g biochar sample was suspened in 50 mL deionized water and sonicated for 30 min).

The thermally decomposed contents of biochars were characterized by the published method (Bushra And Remya 2024b). Before tests, the biochars were placed in the muffle furnace at 110 °C for 24 h to remove moisture. To measure the ash contents, the biochars were combusted in the muffle furnace at 500 °C for 8 h. After cooling down, the ash content was determined by Eq. 2. To measure the volatile matters, the biochars were heated in the muffle furnace at 950 °C for 7 min in an oxygen-free atmosphere. After cooling down, the volatile content was determined by Eq. 3.

$$Ashcontent\% = \frac{Massofashresidue/g}{Massofdrybiochar/g} \times 100 \quad (2)$$

$$Volatilemattercontent\% = \frac{(Massofdrybiochr - Massofresidue)/g}{Massofdrybiochar/g} \times 100 \quad (3)$$

2.3 Water filtration studies with biochar

The biochar samples were ground to pass a sieve with a 500 μm mesh before use. Biochars were soaked in 70 °C DI water, at a ratio of 20 mL per gram of biochar, for 2 h prior to centrifugation. After hot water incubation, the biochar suspension was centrifuged at 1100 × g for 1 h. Finally, the deposits were dried in an oven at 50 °C overnight with constant airflow. The biochar samples without activation were also used for filtration tests as references.

A conical funnel-based filtration system was set up for the filtration tests. Filter papers with varied diameters (12 to 18 cm) to hold varied amounts of biochar (Fisher Scientific, P5 grade, pore size of 20 μm) were used with dimensionally matched funnels. The biochar samples were filled into the filter papers in funnels and tapped firmly to ensure the funnels were fully loaded. The system was gravity-driven, with no external pressure applied. Filtration proceeded at a flow rate of ~ 1.8–2.2 mL/s across the small- and medium-scale funnels. Pressure drop was not directly measured but was minimized by maintaining uniform funnel and filter paper configurations. The variations of biochar loading, volume, and height by filter paper size were summarized in Table 2. Control experiments using P5 filter papers without biochar showed < 0.3% removal of ammonia, confirming that the filter served only as mechanical support and did not contribute measurably to contaminant removal.

Ammonia and polystyrene micro/nanoplastic (PS-MNPs) were selected as the model contaminants to be removed from water by biochar. For the ammonia

Table 2 Parameters of the water filtration system with biochar

The scale of filtration units	Diameter of filter paper (cm)	Funnel volume (cm^3)	Biochar stack height (cm)	Biochar loading (g)
Small (S)	12	84	2.5	7.5
Medium (M)	15	162	3.5	15
Large (L)	18	298	5.5	30

adsorption studies, ammonia solutions with 1 ppm, 10 ppm, and 100 ppm of free ammonia were prepared by diluting concentrated ammonia stock solutions (Arocep Inc., 1000 ppm) with DI water. For each filtration experiment, 50 mL of ammonia solution was poured onto the biochar stack surface and allowed to spread into the biochar and eventually pass through the biochar stacks. The filtrates were collected and measured for the concentration of the remaining ammonia by a multiparameter meter (YSI MultiLab 4010–2, YSI Incorporated, Yellow Springs, Ohio, USA), and the adsorption efficiency of ammonia by biochar samples was calculated by the following equation:

$$\text{Adsorption effiency\%} = \frac{(C_1V_1 - C_2V_2) - (C_1V_1 - C_{Blank}V_{Blank})}{C_1V_1} \times 100 \quad (4)$$

And it can be simplified as

$$\text{Adsorption effiency\%} = \frac{C_{Blank}V_{Blank} - C_2V_2}{C_1V_1} \times 100 \quad (5)$$

where C_1 and C_2 are the concentrations of ammonia solution before and after biochar filtration, V_1 is the initial volume of ammonia solution before filtration, and V_2 is the collected volume after biochar filtration. C_{blank} is the ammonia concentration through the blank filter paper, and V_{Blank} is the collected volume after flowing through blank filter paper.

To investigate the adsorption mechanism of ammonia, biochar samples were collected after filtration experiments with 100 ppm ammonia solutions. The recovered biochars were oven-dried at 60 °C and ground for analysis. FT-IR spectra were recorded on a Nicolet Nexus 470 FT-IR Spectrometer (ATR mode, Thermo Electron Scientific Instruments Corporation, Madison, WI, USA) in the range of 4000–600 cm^{-1} with 32 scans at 16 cm^{-1} resolution. Zeta potential measurements were performed on biochar before and after ammonia adsorption.

The filtration of MNPs was performed similarly to ammonia. Water samples containing PS-MNP (Invitrogen FluoSpheres™, labeled by yellow-green fluorescent 505/515) with four different particle sizes (the average sizes were 0.10, 0.50, 0.95, and 2.10 µm individually) were prepared by following a protocol developed in a previous study (Müller et al. 2020). Briefly, concentrated PS-MNP stock suspensions (1×10^{10} numbers/mL, pH 5.0) were mixed with HPLC-grade water (Thermo Fisher Scientific Inc., Waltham, MA) and ultrasonicated for 1 h to obtain working suspensions containing 2×10^5, 2×10^6, and 2×10^7 numbers/mL. For pH experiments, aliquots of the suspensions were adjusted to pH 5.0, 7.4, or 9.0 using standard buffer solutions (Fisher Scientific). All suspensions were stored at 4 °C until use. Prior to filtration, each suspension was ultrasonicated for 30 min with 300 rpm of stirring to ensure homogeneous distribution of the MNP particles.

The filtration was carried out following the same protocols for the ammonia solutions as mentioned above. After filtration, the fluorescent MNP content was measured using a UV–visible spectrophotometer (SpectraMax 384 Plus Microplate Reader, Molecular Devices, LLC, San Jose, CA, USA) with wavelength λex = 505/ λem = 515 nm. A calibration curve was constructed based on an MNP concentration of 5 µg/mL ($R^2 = 0.9997$). Filtration efficiency for PS-MNPs was calculated as the percentage reduction in particle concentration between the influent suspension and the collected filtrate. Particle concentrations before and after filtration were determined from UV–Vis absorbance at 525 nm using a standard calibration curve (HPLC water as reference). Blank filter paper controls (P5 grade, 20 µm) showed < 0.5% apparent removal, confirming that the support medium did not measurably contribute to MNP retention. The adsorption efficiency of PS-MNPs by biochar was also calculated by the Eq. 5.

Prior to adsorption and filtration experiments, the fluorescent PS-MNPs were also characterized by fluorescence microscopy. A fluorescence microscope (Zeiss LSM880, Carl Zeiss Vision Inc., Blackwood, NJ, USA) equipped with a FITC filter set (λ_ex = 505 nm, λ_em = 515 nm) was used to visualize the yellow-green labeled particles. A 10 µL aliquot of each suspension was drop-cast onto a glass slide, covered with a coverslip, and imaged at 40× magnification. Images were captured with an integrated CCD camera and analyzed using Zen 2.3 SP1 software. This characterization step confirmed the fluorescence and approximate size distribution of the PS-MNPs prior to use. The biochar samples after filtration treatments were also characterized by SEM, BET and zeta

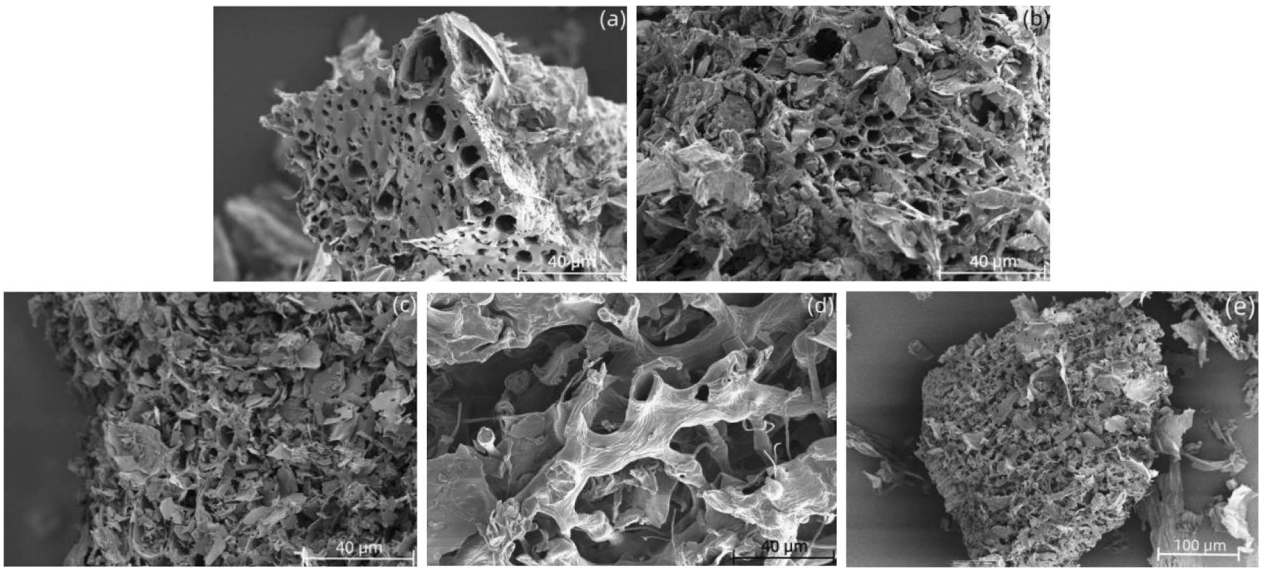

Fig. 1 Scanning electron microscope (SEM) images of biochar representatives. (**a**) Corn cob-based biochars (CCB550), (**b**) Cocoa husk-based biochars (CHB550), (**c**) Walnut shell-based biochars (WSB550), (**d**) Bamboo stalk-based biochars (BSB550), (**e**) Poultry litter-based biochars (PLB). Font color (black or white) was selected based on image background contrast to ensure legibility

potential tests with the same method described before, for the investigation of PS-MNPs adsorption mechanism.

A preliminary regeneration test was conducted to assess the reusability of biochar for ammonia removal. After the initial adsorption experiment with 10 ppm ammonia solution (Cycle 0), the used biochars were collected, oven-dried at 60 °C, and re-pyrolyzed under the same thermal conditions as their original production. The regenerated biochars were then reused (15 g per test) in filtration experiments with 10 ppm ammonia solution (Cycle 1). This procedure was repeated for a total of three regeneration steps, generating results from Cycle 0 through Cycle 3. Adsorption efficiency was measured in the same manner as described above and compared across cycles to evaluate regeneration performance.

To assess potential secondary pollution from biochar, a 24-h static leaching test was conducted using representative biochar samples. In each test, 1.0 g of biochar was immersed in 100 mL of deionized water and gently agitated at room temperature for 24 h. The suspensions were filtered through 0.45 µm membranes, and the supernatants were analyzed by using GC–MS via the same analysis method. These measurements were performed to evaluate the potential release of PAHs into the aqueous phase during filtration.

2.4 Data analysis

In this study, all the measurements, such as the elemental composition, physicochemical properties, and volatile compounds, were performed in triplicate. The practices for preparing biochar samples and filtration studies were also carried out in triplicate. All the results were presented as mean ± standard deviation (unless specifically noted). The results were analyzed using analysis of variance (ANOVA) and post hoc analysis; the difference was considered to be statistically significant when $p < 0.05$. The graphics were made using Origin (OriginPro 2023, OriginLab Corporation, Northampton, MA).

3 Results

3.1 Preparations and characterizations of biochar samples

In this work, a variety of biochars were produced by pyrolysis and gasification using 5 different feedstocks. The obtained biochars possessed a high and broad range of carbon contents, ranging from 67.66% to 86.62% depending on the feedstock type and processing conditions (revealed by the elemental analysis, in Table S2, Supplementary Materials). The biochar products were characterized by the scanning electron microscope (SEM, images were provided in Fig. 1), which indicated that the obtained biochar products among all feedstocks possess a highly porous and multiple-layered microstructure. The structural features were further validated by the Brunauer–Emmett–Teller (BET) tests (shown in Table S5), as discussed in the supplementary materials. The combination of high carbon content and well-developed porosity makes these biochars highly effective candidates for contaminant adsorption and water filtration applications.

The physicochemical properties of the biochars were strongly influenced by both feedstock type and pyrolysis conditions. Bamboo stalk and walnut shell biochars showed the highest yields (up to ~ 46% and 44%, respectively), while corn cob and cocoa husk biochars produced lower yields. Elemental analysis confirmed that higher pyrolysis temperature and longer residence time increased carbon content and aromaticity while reducing hydrogen and oxygen contents, consistent with greater thermal stability. Feedstock choice also dictated composition; for example, poultry litter biochar contained markedly higher mineral levels (Ca, K, P, Fe, and Zn), whereas bamboo biochar exhibited relatively low mineral contents. Notably, corn cob biochar pyrolyzed at 700 °C (CCB700) displayed the highest carbon content of (86.89 ± 1.12)% (Supplementary Information, Table S2), while bamboo biochar (BSB550) exhibited the largest BET specific surface area (77.19 ± 2.07 m^2/g, see Supplementary Information, Table S5). Across all feedstocks, increasing pyrolysis severity reduced yields but enhanced carbonization and mineral retention patterns. These results confirm that both raw material and thermal treatment play critical roles in tuning biochar properties, while detailed data on yield, density, elemental composition, surface area, and mineral contents are provided in the Supplementary Information (Tables S1-S6).

The 16 USEPA-regulated PAHs were quantified across biochars (Table S4). Naphthalene dominated, while other light PAHs (fluorene, phenanthrene) remained < 5 mg/kg, and heavy PAHs (e.g., benzo[a]pyrene) appeared only in trace amounts (< 1.5 mg/kg) in corn and cocoa husk biochars. Feedstock shaped PAH patterns: cocoa husk showed the broadest spectrum, nutshell had elevated acenaphthylene (3.1 mg/kg), and poultry litter exhibited the lowest levels with no heavy PAHs. Higher pyrolysis temperature lowered light but slightly increased heavy PAHs, and longer residence time marginally raised totals. All samples remained below the 12 mg/kg European Biochar Certificate limit, and no PAHs leached after 24 h tests, confirming minimal risk.

Overall, both feedstock type and pyrolysis conditions markedly influenced the yield, carbon content, mineral composition, and structural properties of the resulting biochars. Higher temperatures and longer residence times generally increased carbon stability and surface area but reduced yield and volatile matter. At the same time, these conditions were associated with elevated ash levels and shifts in (PAH) composition, with light PAHs such as naphthalene being most abundant and heavy PAHs present at relatively low concentrations. These findings emphasize the need to optimize processing parameters to balance performance with environmental safety. Comprehensive data, including detailed elemental, mineral, and PAH profiles, are provided in the Supplementary Information (Tables S1-S6).

3.2 Adsorption and filtration studies on contaminants

In the filtration studies, we explored the effectiveness of using these biochar samples to adsorb ammonia and MNPs in water. Control tests using P5 filter paper without biochar showed < 0.3% and < 0.5% removal of ammonia and MNPs respectively, confirming that contaminant removal was attributable to the biochar layer rather than the support medium. Accordingly, removal efficiencies were calculated using the support-corrected equation (Eq. 5), though the correction did not materially affect the values because blank retention was negligible.

Figure 2 and Fig. 3 summarize the removal rates of ammonia from ammonia-containing solutions by funnel filters with different biochar loads or different types of biochar. Bamboo biochar achieved the highest removal of ammonia (55.12%) (Fig. 2a) when the ammonia removal rates by biochar made from different feedstocks were compared at the same pyrolysis conditions. However, the removal rate achieved by bamboo biochar is still significantly lower than the removal rate achieved by biochar produced from poultry litter by gasification (67.62%). When the impacts of biochar activation by hot water incubation were compared for all corn cob biochar samples, a significant increase in removal rate was found for corn cob biochar produced at 350 °C with hot water incubation (Fig. 2b) (Panwar And Pawar 2022). The pyrolysis temperature was a significant factor for ammonia removal rate. Though all three corn cob biochar samples demonstrated at least a 35% removal rate, CCB700 achieved greater removals of ammonia than CCB550 and CCB350 (Fig. 2b). Figure 3a shows the removal rate of ammonia from solutions containing 1 ppm to 100 ppm ammonia by corn biochar samples. Overall, CCB700 achieved higher ammonia removal rates, especially for solutions with high levels of ammonia; the removal rates were significantly higher than those achieved by CCB350 and CCB550.

Also, the level of ammonia in the solutions before filtration can influence the removal rates significantly (Fig. 3a). In a less concentrated solution (1 ppm), all biochars can adsorb more than 65% of ammonia from the solution, but when increasing the concentration of ammonia to 10 ppm and 100 ppm, the removal rates had all been compromised. At 10 ppm, CCB700 could still maintain a removal rate greater than 60%, however, the removal rates achieved by CCB550 and CCB350 reduced to 46.48% and 40.93%, respectively. At 100 ppm, all biochar samples showed reduced adsorption, as the ammonia removal rates significantly decreased to less than 35%. The effects of biochar loading in the funnel filters

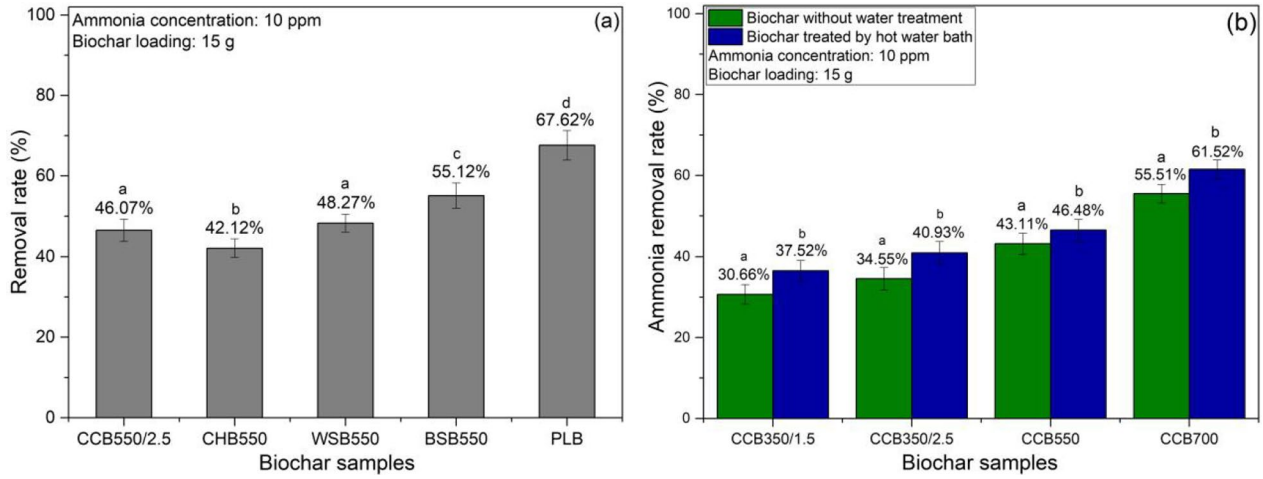

Fig. 2 Removal of ammonia by biochar samples at an initial ammonia concentration of 10 ppm and a biochar loading of 15 g. (**a**) Removal rates of 10 ppm ammonia solution (50 mL) by biochars derived from different feedstocks, including corn cob, cocoa husk, walnut shell, bamboo, and poultry litter, different letters within each biochar sample indicate statistically significant differences. (**b**) Effect of hot-water activation on biochars (three corn biochars as representative), where different letters within each biochar group indicate statistically significant differences. Data are presented as mean ± SD (n = 9), and error bars indicate standard deviations. Statistical differences were determined using Tukey's HSD test ($p < 0.05$). Acronyms for biochar samples are defined in Table S1 (Supplementary Information)

on the ammonia adsorption were found to vary in different cases associated with ammonia concentration. With moderate ammonia concentrations (10 ppm, Fig. 3b), higher CCB550 loads resulted in significantly increased ammonia adsorption. With the load increased from 7.5 g to 15 g and then to 30 g, the removal rates improved from 37.60% to 46.48%, and then reached 56.07%, accordingly. For CCB700, a significant increase in the removal rate was found between 7.5 g and 15 g of biochar loads (from 43.56% to 61.52%). However, when the biochar load increased to 30 g, the removal rate increased (at 63.95%) but not significantly. For CCB350, the adsorption did not increase significantly until the biochar load increased from 7.5 g to 30 g. On the other hand, with a low-concentration solution (1 ppm) being filtered by biochar, the biochar loading was not a significant factor. However, with higher concentrations of test ammonia (10 ppm and 100 ppm) in the solutions, increased biochar load improved the adsorption or removal rates of ammonia (Fig. 3c).

Using the same filtration setups, water containing PS-MNPs was filtered to evaluate the capability of corn biochar as an adsorbent for MNPs. In general, different biochars showed the capacity of removing MNPs from water (Fig. 4a). In the following tests on corn biochars, CCB550 and CCB700 possessed high adsorption capacities with > 90% removal rates for MNP samples with different sizes and concentrations. For CCB350, adsorption of MNPs was affected by various factors, including the size and concentration of MNPs, and the biochar loading. As shown in Fig. 4(b), CCB350 effectively adsorbed the larger-sized (0.95 μm and 2.10 μm, at 2×10^6/mL) PS-MNPs, achieving > 90% removal rates. Whereas, for the smaller-sized PS-MNPs (0.5 μm and 0.1 μm), the removal rate of 0.5 μm particles achieved by CCB350 was reduced to 65.54%, and for the 0.1 μm particles, the removal rate was down to 16.84%. Also, the adsorption capabilities of CCB350 were impacted by the concentration of MNPs (Fig. 5a and b). For example, for the filtration of solutions containing 0.95 μm or 2.1 μm PS-MNPs by 15 g of CCB350, the removal rates were maintained at high levels (> 90%) for both 2×10^5/mL and 2×10^6/mL of PS-MNPs. But for solutions with 2×10^7/mL PS-MNPs, the adsorption was compromised, and the removal rates for 0.95 μm and 2.1 μm PS-MNPs dropped to 84.6% and 79.7%, respectively.

It was also found that increasing the biochar load can improve the adsorption effectiveness of CCB350. While CCB550 and CCB700 achieved similar removal rates regardless of the biochar loads, the removal of MNPs by CCB350 showed dependency on the biochar load. With the amount increased from 7.5 g to 15 g and to 30 g, the adsorption and removal of MNPs significantly increased (Fig. 6a). Such an improvement in the removal rate was found for filtering MNPs with different sizes. For MNPs with a 0.5 μm particle size, the removal rate was only 48.82% with 7.5 g of biochar load. Whereas, when the biochar load was increased to 15 g, the removal rate was significantly improved to 65.54%, and further improved to 77.18% with 30 g of

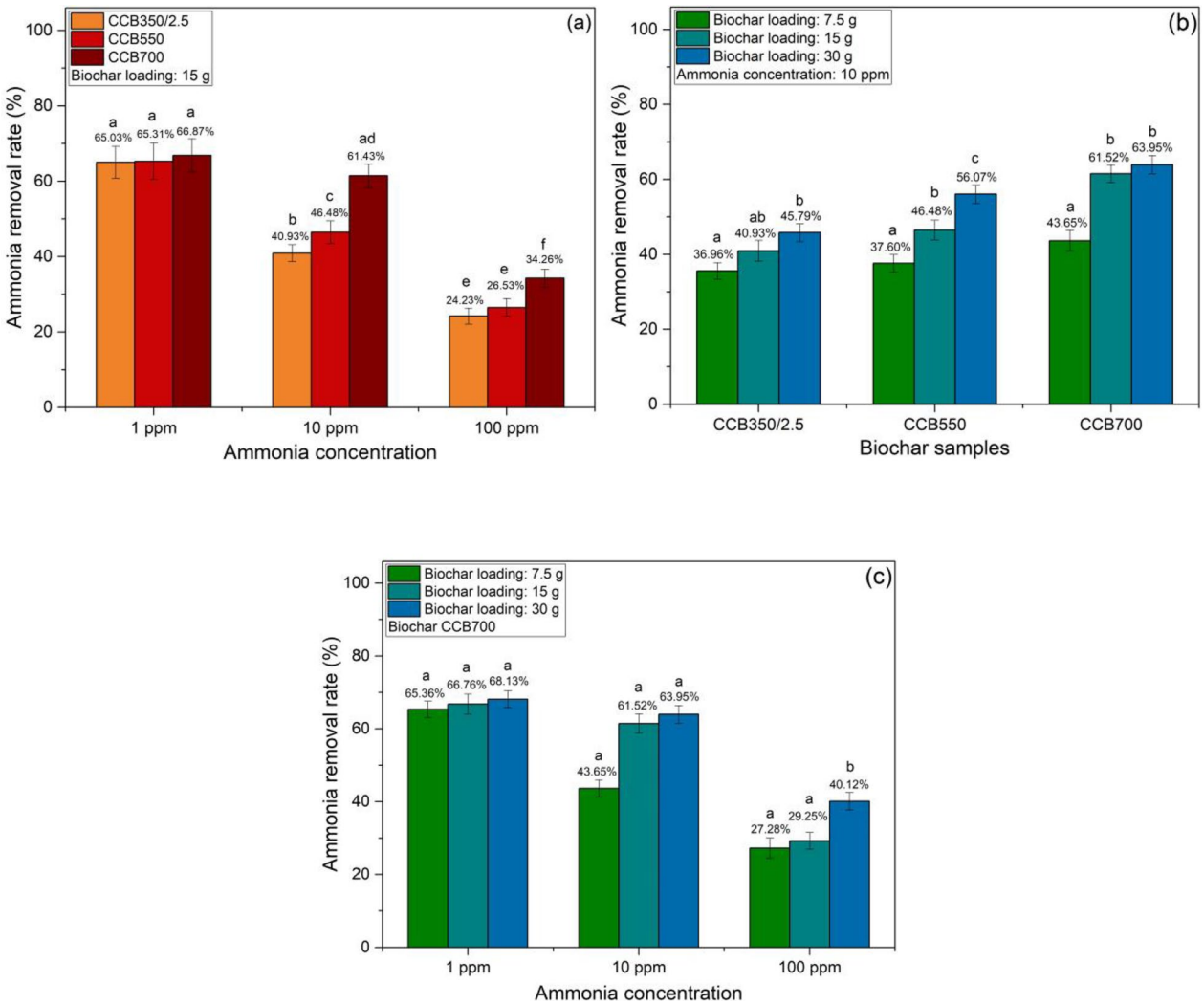

Fig. 3 Influence of process parameters on ammonia removal by biochars (corn biochars as representative). (**a**) Effect of initial ammonia concentration (1, 10, and 100 ppm) on removal efficiency; different letters indicate significant differences among all treatments. (**b**–**c**) Effect of biochar loading (7.5, 15, and 30 g) on ammonia removal efficiency, where different letters indicate significant differences within the same treatment group. Data are presented as mean ± SD (n = 9), and error bars indicate standard deviations. Statistical differences were determined using Tukey's HSD test ($p < 0.05$)

biochar load (Fig. 6b). Similarly, when filtering high-concentration MNP solutions (2×10^6 particles/mL and 2×10^7 /mL), with 7.5 g of CCB350, the removal rates were 79.9% and 72.05%, respectively. After increasing the biochar load to 30 g, the removal rates could reach 93.25% and 89.12%, respectively (Fig. 6c). The significance of PS-MNPs removal by biochar could be illustrated by the fluorescent microscopy images shown in Fig. 7. After filtration, much fewer particles (green dots) were found in the filtrates comparing the solution before filtration.

In addition to removal efficiency, potential release of polycyclic aromatic hydrocarbons (PAHs) from biochar into the filtrates was examined by 24-h leaching tests. GC–MS analysis of the 16 EPA priority PAHs confirmed that none were detectable in any filtrates from the tested biochars. These findings demonstrate that short-term aqueous filtration with biochar did not introduce measurable PAHs, indicating negligible risk of secondary contamination.

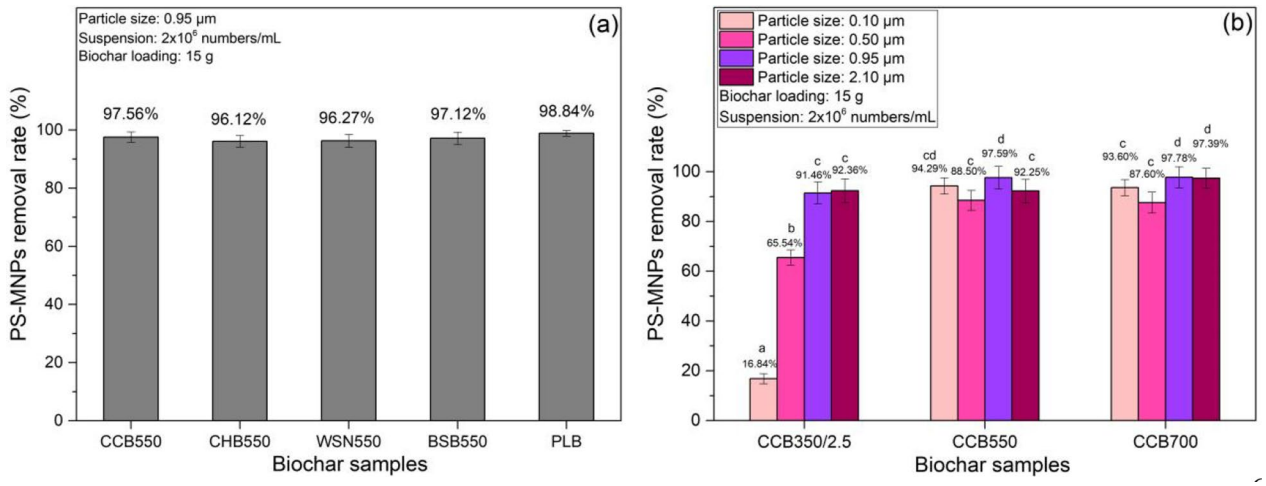

Fig. 4 Removal of PS-MNPs by biochar samples at particle concentration of 2×10^6 particles/mL. (**a**) Effect of biochar feedstock type on removal efficiency (0.95 μm PS-MNPs at 15 g biochar loading). (**b**) Effect of particle size (0.10–2.10 μm) on removal efficiency (corn biochars as representative) at 15 g loading. Data are presented as mean ± SD (n = 9), and error bars indicate standard deviations. Statistical differences were determined using Tukey's HSD test ($p < 0.05$). Different letters indicate significant differences among all treatments

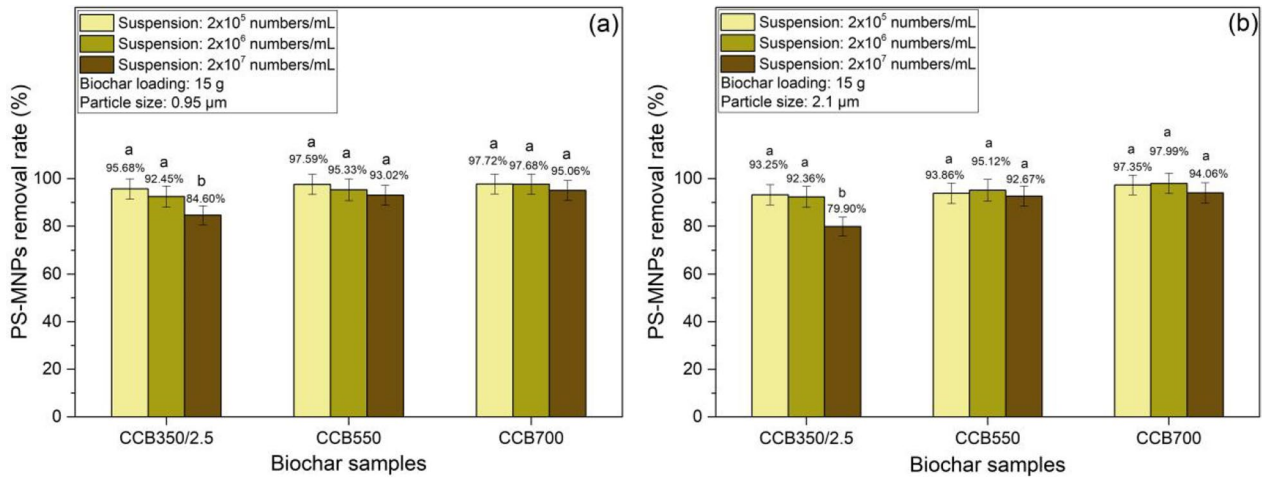

Fig. 5 Effect of suspension concentration on the removal of PS-MNPs by biochars (corn biochars as representative, 15 g loading). (**a**) Removal efficiencies of 0.95 μm PS-MNPs at three suspension concentrations (2×10^5–2×10^7 numbers/mL). (**b**) Removal efficiencies of 2.1 μm PS-MNPs under the same concentration conditions. Data are presented as mean ± SD (n = 9), and error bars indicate standard deviations. Statistical differences were determined using Tukey's HSD test ($p < 0.05$). Different letters indicate significant differences among all treatments

3.3 Adsorption mechanism studies

To investigate adsorption mechanisms of biochars across different contaminant types, this study examined ammonia and PS-MNPs as representative targets. Given their distinct physicochemical properties, mechanistic investigations were carried out separately for each contaminant using appropriate analytical approaches."

3.3.1 Ammonia adsorption mechanism

Because the experimental solutions were prepared at neutral pH, ammonia was present predominantly as ammonium ions (NH_4^+), which are cationic and can interact electrostatically with negatively charged biochar surfaces. FT-IR spectroscopy was used to examine the surface functional group changes of CCB550 biochar before and after filtration of 100 ppm ammonia solution (Fig. 8). In the O–H stretching region (~3200–3500 cm^{-1}), the band broadened and became more intense after adsorption, indicating stronger hydrogen bonding (Smith 1999). In the carbonyl region, the pristine sample showed a band at 1688 cm^{-1}, which disappeared after adsorption and was replaced by new peaks

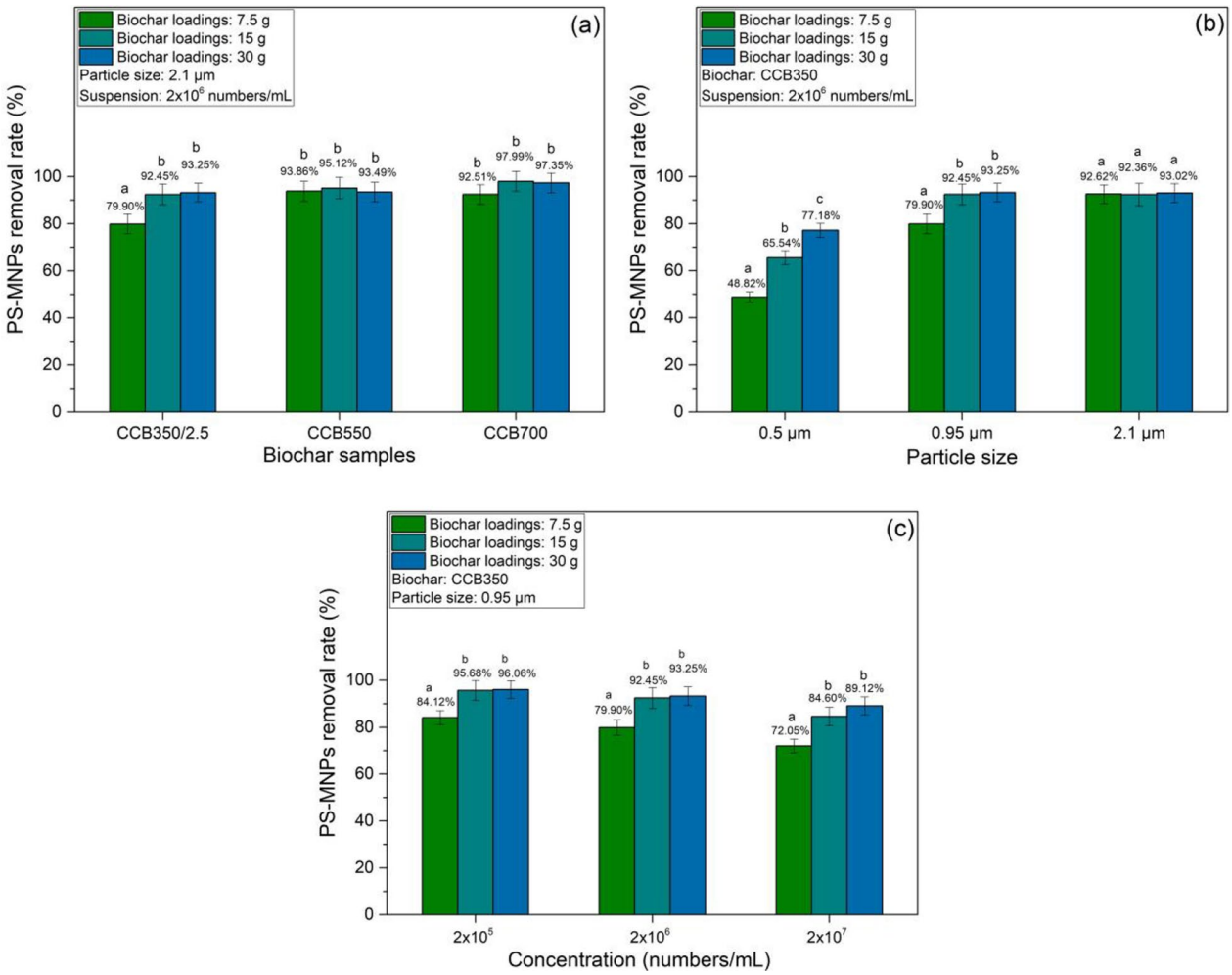

Fig. 6 Effects of biochar loadings (corn biochars as representative) on the removal of PS-MNPs. (**a**) Removal efficiencies of 2.1 μm PS-MNPs (2×10^6 numbers/mL) at biochar loadings of 7.5, 15, and 30 g. (**b**) Effect of biochar loading on PS-MNP removal at different particle sizes (0.5, 0.95, and 2.1 μm) using CCB350 under identical suspension conditions. (**c**) Effect of biochar loading on the removal of 0.95 μm PS-MNPs across suspension concentrations of (2×10^5 to 2×10^7 numbers/mL) particles/mL using CCB350. Data are presented as mean ± SD (n = 9), and error bars indicate standard deviations. Statistical differences were determined using Tukey's HSD test ($p < 0.05$). Different letters indicate significant differences within the same treatment group

at 1648 and 1616 cm^{-1}. These shifts are plausibly associated with hydrogen-bonded carbonyls and asymmetric COO^- stretching, suggesting reorganization of carboxyl groups during NH_4^+ interaction (Chen et al. 2008). In the 1400–1500 cm^{-1} region, two bands were present at 1437 and 1379 cm^{-1} in the pristine biochar, assigned to symmetric COO^- stretching(Nair et al. 2022). After ammonia adsorption, these bands shifted to 1400 and 1370 cm^{-1}, consistent with COO^- groups participating in outer-sphere complexation with NH_4^+ ions, with possible overlap from NH_4^+ deformation. Additionally, a new band emerged at 1018 cm^{-1}, attributable to C–O stretching of phenolic or carboxyl-related groups (with possible contributions from Si–O vibrations in the ash fraction) (Zhang et al. 2021).

Zeta potential analysis further confirmed the role of electrostatic interactions during ammonia adsorption (Table 3). All pristine corn biochars carried negative ζ-potentials, with values of -29.86 ± 1.89 mV for CCB350/2.5, -25.73 ± 1.48 mV for CCB550, and -24.65 ± 1.76 mV for CCB700. After exposure to 100 ppm ammonia solution, the ζ-potentials of all samples shifted toward less negative values: -22.43 ± 1.89, -18.72 ± 1.35, and -17.73 ± 1.48 mV, respectively. The reductions of 7–8 mV indicate partial charge neutralization of the biochar surfaces by adsorbed NH_4^+ ions. Tukey's HSD test ($p < 0.05$) confirmed that

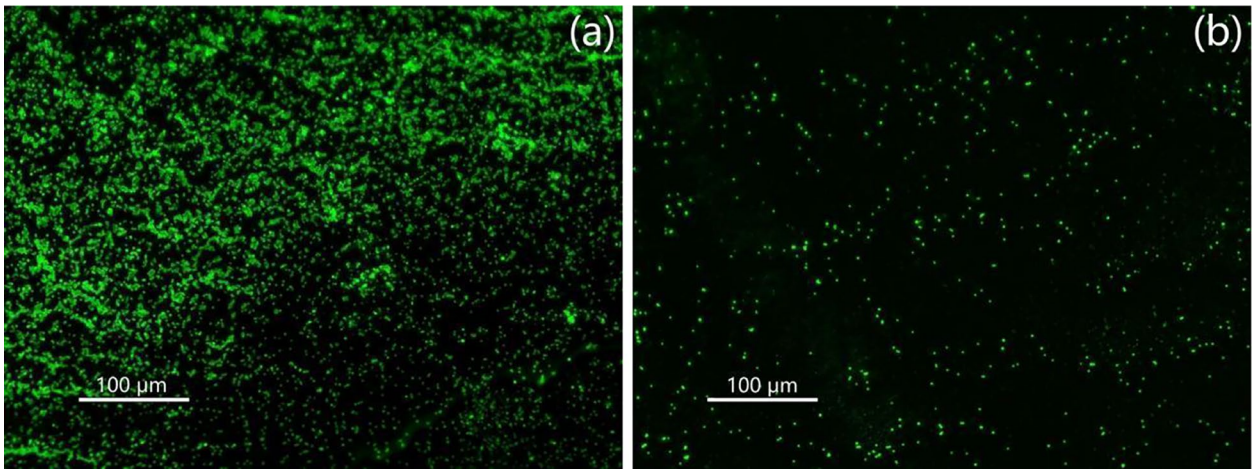

Fig. 7 Fluorescent microscope images of PS-MNPs suspensions (2.1 μm, 2×10^7 numbers/mL). (**a**) Before filtration, (**b**) After filtration by 15 g of CCB700. Green dots: Labeled PS-MNPs

these shifts were statistically significant. Among the samples, the largest change was observed for CCB350/2.5, while CCB700 also exhibited a pronounced shift, consistent with its higher removal efficiency.

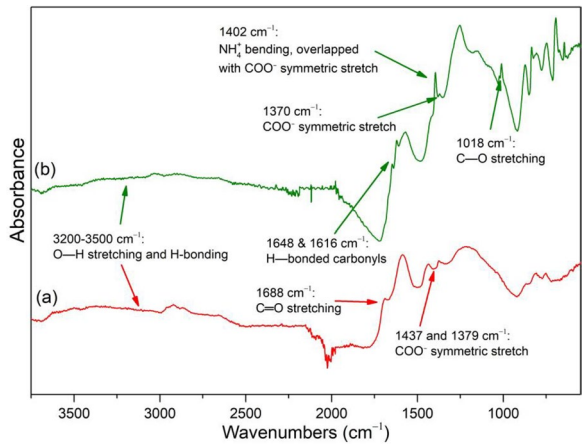

Fig. 8 FT-IR spectra of CCB550 before (**a**) and after (**b**) filtration of 100 ppm ammonia solution

Table 3 Zeta potentials of corn biochars before and after the adsorption of ammonia

Biochar sample	Zeta potential before adsorption (mV)	Zeta potential after adsorption (mV)
CCB350/2.5	-29.86 ± 1.89^a	-22.43 ± 1.89^b
CCB550	-25.73 ± 1.48^a	-18.72 ± 1.35^b
CCB700	-24.65 ± 1.76^a	-17.73 ± 1.48^b

* The results are presented as mean ± SD on dry basis, where n = 9. Tukey's HSD test was used to determine the statistical difference ($p < 0.05$). The mean value accompanied by different letters indicates significant differences among all samples in the same row

** The concentration of ammonia: 100 ppm, the biochar loadings in the tests: 15 g

3.3.2 PS-MNPs adsorption mechanism

To investigate the PS-MNPs adsorption mechanism, the microstructures of corn biochar samples after PS-MNPs filtration tests were investigated by SEM. The SEM images of the surface of biochar samples after filtering 0.95 μm PS-MNPs (Fig. 9a) and 2.1 μm PS-MNPs (Fig. 9b) are shown. PS-MNPs on the surface of biochar layers (green arrows) were observed, and the image shows that the MNPs firmly stacked in multiple layers on the surfaces of biochar contributed to the adsorption by stacked layer trapping and retaining the contaminants, especially with large sizes. The porous structure of biochar was another contributor to adsorbing MNPs. As shown in Fig. 9(c), after filtration, the pores were partially or completely filled with PS-MNPs (green arrows), indicating that the pore structures can contribute to the adsorption of biochars. The observations were supplemented by BET tests of the biochar samples (Table 4). After filtering PS-MNPs, the pore volume of the biochar samples significantly reduced, indicating portions of the MNPs were adsorbed or trapped by the pores. It was also found that some portions of PS-MNPs were adherent or attached to the outside layer of porous microstructure (Fig. 9d, green arrow) during the treatment. This could be explained by the electrostatic attractions between biochars and PS-MNPs. Though polystyrene materials typically have a negatively charged surface (negative zeta potential), in this study, PS-MNPs prepared in acidic suspension would show a positively charged surface, and the biochars had a negatively

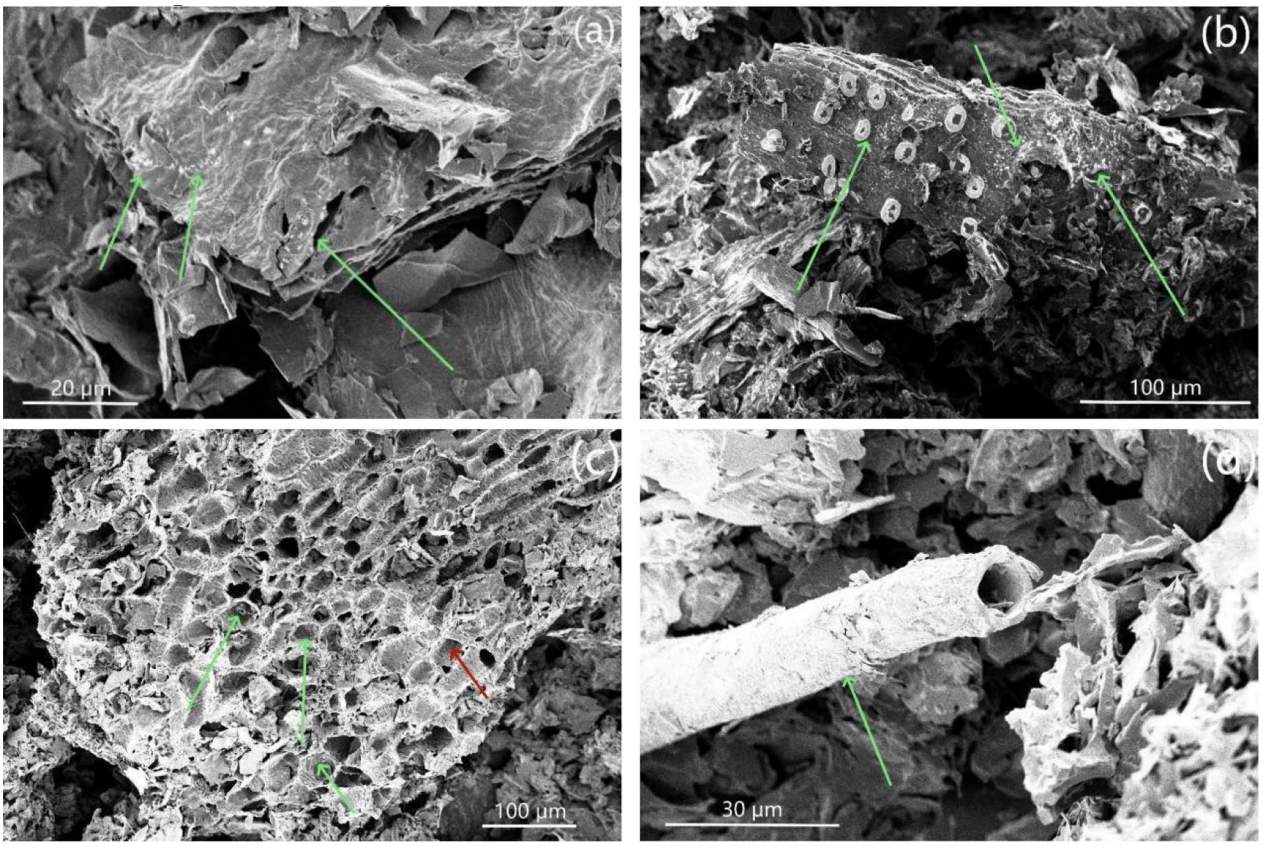

Fig. 9 Representative SEM images of CCB550 after the adsorption of PS-MNPs. (**a**). Treatment of 0.95 μm PS-MNPs; (**b**), (**c**), (**d**). Treatment of 2.1 μm PS-MNPs

Table 4 Total pore volumes of corn biochars before and after the adsorption of PS-MNPs

Biochar sample	Total pore volume before adsorption (cm^3/g)	Total pore volume after adsorption (cm^3/g)
CCB350/2.5	0.01252 ± 0.00029^a	0.00046 ± 0.00007^b
CCB550	0.02793 ± 0.00041^a	0.01027 ± 0.00010^b
CCB700	0.02317 ± 0.00022^a	0.00981 ± 0.00011^b

* The results are presented as mean ± SD on a dry basis, where n = 9. Tukey's HSD test was used to determine the statistical difference ($p < 0.05$). The mean value accompanied by different letters indicates significant differences among all samples in the same row

** The concentration of PS-MNPs: 2×10^7 numbers/mL, the average size: 2.1 μm, the biochar loadings in the tests: 15 g,

Table 5 Zeta potentials of corn biochars before and after the adsorption of PS-MNPs

Biochar sample	Zeta potential before adsorption (mV)	Zeta potential after adsorption (mV)
CCB350/2.5	-29.86 ± 1.89^a	-17.44 ± 1.09^b
CCB550	-25.73 ± 1.48^a	-12.69 ± 1.13^b
CCB700	-24.65 ± 1.76^a	-10.45 ± 1.01^b

* The results are presented as mean ± SD on dry basis, where n = 9. Tukey's HSD test was used to determine the statistical difference ($p < 0.05$). The mean value accompanied by different letters indicates significant differences among all samples in the same row

** The concentration of PS-MNPs: 2×10^7 numbers/mL, the average size: 2.1 μm, the biochar loadings in the tests: 15 g

charged surface. Due to the electrostatic effect, the PS-MNPs could be attracted by the biochars and adhere to the outer layer. Table 5 shows that after filtering PS-MNPs, the zeta potentials of biochars became less negative, which further indicated electrostatic attraction between the two.

To further verify this mechanism, adsorption experiments were conducted under different pH conditions (Table 6). Across all corn biochars, removal efficiency was highest at pH 5.0, moderate at near-neutral pH (7.4), and lowest at pH 9.0. For example, CCB700 achieved 94.06 ± 3.12% removal at pH 5.0, compared with 84.60 ± 1.77% at pH 7.4 and 76.18 ± 2.05% at pH 9.0. Similar trends were observed for CCB550 (92.67 ± 2.89%, 87.45 ± 2.01%, and 76.05 ± 1.98% at pH 5.0, 7.4, and 9.0, respectively) and CCB350/2.5 (79.90 ± 2.25%,

Table 6 Adsorption efficiency of PS-MNPs by corn biochars at different pH values

Biochar sample	MNPs adsorption efficiency/%		
	pH 5.0	pH 7.4	pH 9.0
CCB350/2.5	79.90 ± 2.25^{a}	72.52 ± 1.40^{b}	58.07 ± 1.66^{c}
CCB550	92.67 ± 2.89^{a}	87.45 ± 2.01^{b}	76.05 ± 1.98^{c}
CCB700	94.06 ± 3.12^{a}	84.60 ± 1.77^{b}	76.18 ± 2.05^{c}

* The results are presented as mean ± SD on dry basis, where n = 9. Tukey's HSD test was used to determine the statistical difference ($p < 0.05$). The mean value accompanied by different letters indicates significant differences among all samples in the same row

** The concentration of PS-MNPs: 2×10^{7} numbers/mL, the average size: 2.1 μm, the biochar loadings in the tests: 15 g

Table 7 Regeneration performance of corn biochars

Biochar sample	Adsorption efficiency (%) against 10 ppm of ammonia			
	Cycle 0	Cycle 1	Cycle 2	Cycle 3
CCB350/2.5	40.93 ± 1.44^{a}	40.96 ± 1.22^{a}	38.63 ± 1.16^{b}	33.68 ± 1.03^{c}
CCB550	46.48 ± 1.33^{a}	45.72 ± 1.17^{a}	43.19 ± 1.28^{ab}	40.88 ± 1.15^{b}
CCB700	61.43 ± 2.29^{a}	60.09 ± 1.36^{a}	58.72 ± 1.39^{a}	55.41 ± 1.04^{b}

* The results are presented as mean ± SD on dry basis, where n = 9. Tukey's HSD test was used to determine the statistical difference ($p < 0.05$). The mean value accompanied by different letters indicates significant differences among all samples in the same row

** Cycle 0 refers to fresh biochar; Cycles 1–3 represent sequential regeneration by re-pyrolysis and reuse

72.52 ± 1.40%, and 58.07 ± 1.66%). These pH-dependent patterns confirm that electrostatic interactions are central to MNP adsorption: protonation at low pH reduces repulsion and enhances adhesion, while increased negative charges at alkaline pH promote electrostatic repulsion and lower adsorption efficiency.

3.4 Regeneration performance

The reusability of biochar filters was evaluated through repeated adsorption–regeneration cycles using 15 g of material against 10 ppm ammonia solution. After the initial adsorption with fresh biochars (Cycle 0), the used samples were re-pyrolyzed under identical conditions and reused for three additional cycles (Cycles 1–3). The adsorption efficiencies are summarized in Table 7. All three corn cob biochars retained high ammonia removal efficiencies across multiple regenerations, with only gradual declines observed over successive cycles. CCB350/2.5 remained stable between Cycle 0 (40.93 ± 1.44%) and Cycle 1 (40.96 ± 1.22%), but declined significantly in Cycle 2 (38.63 ± 1.16%) and Cycle 3 (33.68 ± 1.03%). CCB550 showed a similar pattern, starting at 46.48 ± 1.33% in Cycle 0 and remaining statistically unchanged in Cycle 1 (45.72 ± 1.17%), before decreasing to 43.19 ± 1.28% and 40.88 ± 1.15% in Cycles 2 and 3. The high-temperature CCB700 exhibited the greatest regeneration stability, with efficiencies statistically unchanged through Cycle 2 (61.43 ± 2.29% to 58.72 ± 1.39%) and only a modest decline by Cycle 3 (55.41 ± 1.04%).

These results demonstrate that thermal re-pyrolysis can effectively restore adsorption activity, enabling biochar reuse over multiple cycles with limited performance loss. In particular, CCB700 exhibited superior regeneration stability compared with lower-temperature biochars, underscoring the role of pyrolysis conditions in determining long-term reusability. This provides preliminary but strong evidence that regeneration is a feasible strategy to extend the service life of biochar filters and enhance their sustainability for water treatment applications.

4 Discussion

Water contamination by ammonia and emerging pollutants such as micro/nanoplastics (MNPs) presents a pressing global challenge for environmental protection and public health. Conventional treatment processes often face limitations in efficiency, cost, or secondary pollution risks, creating a strong demand for low-cost and sustainable alternatives. Biochar, produced from biomass under oxygen-limited pyrolysis, has been proposed as a sustainable adsorbent. However, the adsorption performance of biochar is strongly dependent on its physicochemical properties, including pore structure, surface functional groups, and mineral content, which remain insufficiently understood under realistic filtration conditions. In this study, we systematically evaluated the capacity of diverse biochars to remove ammonia and MNPs from water, and further investigated the underlying mechanisms. The following discussion interprets these findings in relation to material characteristics, adsorption pathways, and broader implications for water treatment applications.

4.1 Characteristics of biochar affecting adsorption efficiency

Our biochar samples showed promising efficacy in removing ammonia and MNPs from water sources, and the removal capacities varied by the type of biochar, properties of contaminants, and filtration conditions. Biochars prepared from various feedstocks effectively adsorbed ammonia from aqueous solutions, with performance depending on the type of biochar and the amount of biochar used in the filters, as well as the initial ammonia concentration of the solutions. Among the three types of corn biochars in the following tests, CCB700 (pyrolyzed at 700 °C) exhibited the highest ammonia adsorption capacity. This result aligns with its elevated carbon content (Table S2), reflecting greater aromaticity

and thermal stability that strengthen interactions with ammonia. Similar trends have been observed in previous studies, where highly pyrolyzed biochars showed enhanced nutrient ions adsorption (such as ammonium and phosphate), largely due to increased aromatic condensation and reduced volatile contents (Thomas et al. 2020; Abbas et al. 2018; Ahmad et al. 2014). In contrast, bamboo stalk biochar at 550 °C (BSB550) exhibited the largest BET surface area, suggesting a greater potential for physical adsorption of particulate species such as MNPs through pore-filling and surface entrapment. Such surface-area-driven mechanisms for micro/nanoplastic capture have also been reported for porous carbonaceous materials in recent work (Ravindiran et al. 2024; Kalsoom et al. 2024). These distinctions illustrate how different structural features can favor different adsorption pathways. These distinctions illustrate how structural features guide adsorption pathways. Furthermore, the observed dependence on pyrolysis temperature is consistent with earlier findings that carbon content, surface area, pore structure, and cation exchange capacity are strongly temperature-dependent and together determine biochar adsorption performance.

4.2 Adsorption of ammonia: performance and mechanism

The ammonia filtration studies revealed that the adsorption efficiency of biochar was impacted by the initial concentration of ammonia in the solutions. With lower ammonia concentrations (1 ppm), all three biochar samples achieved comparable removal rates. As the ammonia concentration increased to 10 ppm, the adsorption capacities diverged, with CCB700 maintaining the highest removal rate even at higher concentrations (60% at 10 ppm). In contrast, the removal rates for CCB550 and CCB350 decreased notably under the same conditions. At 100 ppm, the adsorption capacity of the biochars was diminished, leading to reduced ammonia removal rates. This can be attributed to the saturation of the biochar's active adsorption sites. Like other adsorbents, biochar possesses a finite number of surface sites available for ammonia binding. At low concentrations (e.g., 1 ppm), these sites can readily accommodate ammonia molecules, resulting in high adsorption efficiency. However, as the ammonia concentration increases, the number of available binding sites becomes limited. Once saturation is reached, additional ammonia molecules cannot be effectively adsorbed, leading to a plateau or decline in removal efficiency. In the case of the 100 ppm ammonia solution, it is likely that the biochar's surface area and active sites are no longer sufficient to capture excess ammonia, resulting in reduced adsorption performance. Furthermore, at higher concentrations, competition among ammonia molecules for limited binding sites may further diminish overall efficiency. This behavior aligns with typical adsorption dynamics, where the extent of contaminant removal is governed by both the contaminant concentration and the availability of functional binding sites on the adsorbent (Ghodszad et al. 2021). Our results are consistent with typical adsorption dynamics, where removal efficiency depends on both contaminant concentration and available functional sites (Cai et al. 2023).

The biochar load in the filter is another influential factor for the effectiveness of ammonia adsorption. At lower initial ammonia concentrations (1 ppm), the influence of biochar loading on removal efficiency was minimal. Because the concentration of ammonia was already low, the available adsorption sites on the biochar were not saturated, allowing for relatively high removal efficiency even at lower biochar loadings. However, at higher concentrations (10 and 100 ppm), an increase in biochar amount generally enhanced ammonia removal. Specifically, both CCB550 and CCB700 demonstrated a clear dose-dependent relationship, with higher biochar loading leading to improved removal efficiency. This improvement can be attributed to the increased number of active adsorption sites provided by the additional biochar, as well as enhanced contact between ammonia molecules and the biochar surface, facilitating more effective adsorption. In contrast, CCB350 showed a weaker response to increased loading, with limited improvement in ammonia removal even at a loading of 30 g. This suggests that CCB350 possesses a lower intrinsic adsorption capacity compared to CCB550 and CCB700, likely due to its lower carbon content, reduced porosity, and lower cation exchange capacity (CEC) (Table S6).

Although the results indicate that increasing biochar loading is generally an effective strategy for enhancing adsorption performance, the improvement is not always linear and may become less significant beyond a certain threshold-for example, at 30 g of CCB700. These diminishing returns can be attributed to several factors. As the concentration of biochar increases, adsorption sites may become saturated, limiting the material's ability to capture additional ammonia. Moreover, excessive biochar can lead to particle aggregation or stacking, which reduces the effective surface area and restricts the diffusion of ammonia molecules. Higher loadings may also increase solution viscosity, slowing molecular movement and potentially creating uneven dispersion of biochar, further impeding contact with contaminants. These findings highlight the importance of optimizing both biochar type and dosage to maximize adsorption efficiency while avoiding excessive and unnecessary material usage. This trend aligns with previous reports that have also emphasized the influence of pyrolysis conditions and physicochemical properties on ammonia removal. For example,

Abbas et al. reported that higher-pyrolyzed biochars exhibited increased surface area and cation exchange capacity, resulting in greater ammonia removal (Abbas et al. 2018). Similarly, Lu et al. demonstrated that surface functionalization of biochars enhanced nutrient uptake, emphasizing the role of physicochemical properties (Lu et al. 2020; Goswami et al. 2022). However, compared with these studies, our work systematically links pyrolysis temperature, contaminant concentration, and biochar application rate under filtration conditions, providing a more application-oriented perspective for practical water treatment systems.

Beyond the influence of biochar loading, the physical dimension of biochar particles also plays a role in determining adsorption performance by modifying surface accessibility and contaminant interaction. While the intrinsic pore structure and surface chemistry are largely governed by pyrolysis conditions, particle size reduction can accelerate adsorption kinetics by exposing more accessible surface area. Future work could systematically investigate how particle size distribution affects adsorption dynamics.

To better understand the mechanisms behind the observed performance trends, FT-IR and zeta potential analyses were conducted on representative corn cob biochars. Under the experimental pH, aqueous ammonia existed primarily as ammonium ions (NH_4^+), which are cationic and electrostatically attracted to negatively charged biochar surfaces. FT-IR spectra revealed clear changes in oxygenated functional groups after ammonia adsorption. Broadening of the O–H stretching band (~3200–3500 cm^{-1}) and the emergence of new peaks at 1648 and 1616 cm^{-1} indicated stronger hydrogen bonding and reorganization of carboxyl groups. Shifts of carboxylate bands from 1437 and 1379 cm^{-1} to 1400 and 1370 cm^{-1} were consistent with outer-sphere complexation between NH_4^+ and deprotonated carboxylates, while the appearance of a new band at 1018 cm^{-1} suggested activation of C–O functional groups. Complementary zeta potential measurements showed that all biochars were negatively charged under the experimental pH, and that their surface charges shifted toward less negative values after adsorption, reflecting partial neutralization by NH_4^+ ions. Together, these spectroscopic and electrokinetic results demonstrate that ammonia removal involved electrostatic attraction and hydrogen bonding with oxygenated groups. In addition, previous studies have shown that ion exchange between NH_4^+ and exchangeable cations (e.g., K^+, Ca^{2+}, Na^+) in the ash fraction may also contribute, particularly in biochars with higher mineral content, though this pathway was not directly investigated in the present work (Ambaye et al. 2021; Qiu et al. 2023).

4.3 Adsorption of MNPs: performance and mechanism

The notable capability of adsorbing MNPs from water using biochar was also validated in this study. The biochar pyrolysis temperature significantly impacted the adsorption of MNPs by filtration. CCB550 and CCB700 achieved high removal efficiencies (~90%) regardless of the size of MNPs, the concentration of MNPs, and the biochar load in the filters. These findings suggest that higher pyrolysis temperatures enhance biochar properties beneficial for PS-MNP removal. This improvement can be attributed to increased surface area, improved porosity, and enhanced surface chemistry, such as CEC. The consistent performance of these high-temperature biochars across varying PS-MNP sizes and concentrations demonstrates their robustness under diverse filtration conditions, highlighting their promising potential for water purification applications. Similar results have been reported in previous studies where high-temperature biochars exhibited superior performance in removing microplastics and other particulate pollutants. For instance, Anand et al. reviewed microplastic removal technologies and noted that adsorbents with larger surface areas and stable pore structures were more effective at trapping submicron plastics (Anand et al. 2023). Likewise, Poerio et al. emphasized that microplastic capture efficiency is closely linked to adsorbent porosity and surface functionality, echoing the trends observed in our work (Poerio et al. 2019). Compared with these studies, our findings not only confirm the importance of pyrolysis temperature in enhancing structural properties but also highlight that biochars prepared at ≥ 550 °C provide consistently high retention across diverse particle sizes, underscoring their potential for innovation and scalability in water treatment applications.

In contrast, CCB350 exhibited more selective adsorption behavior, showing high removal efficiency for larger PS-MNPs (0.95 μm and 2.1 μm) but significantly lower efficiency for smaller particles (0.5 μm and 0.1 μm). This size-dependent trend suggests that larger particles were more effectively removed through layer trapping and pore-filling. By comparison, smaller particles exhibited weaker interactions and limited retention within the biochar matrix produced at the lowest pyrolysis temperature. Additionally, at elevated PS-MNP concentrations (2×10^7 particles/mL), the adsorption capacity of CCB350 declined, likely due to site saturation or competitive interactions among particles-similar to the behavior observed in ammonia treatment.

A similar trend regarding biochar loading was observed in the treatment of PS-MNPs. While CCB550 and CCB700 exhibited some diminishing returns at higher loadings, CCB350 demonstrated a more pronounced usage-dependent improvement. For instance, when

treating small-sized PS-MNPs (e.g., 0.5 μm) or highly concentrated suspensions (2×10^7 particles/mL), increasing the CCB350 loading from 7.5 g to 30 g significantly enhanced removal efficiency. This suggests that although CCB350 is inherently less efficient than CCB550 and CCB700 at lower loadings, its performance can be substantially improved by increasing the dosage in filtration systems. This trend can be attributed to several factors related to the adsorption mechanisms and structural properties of CCB350. As previously noted, CCB350 has a lower carbon content, less developed porosity, and reduced CEC compared to its higher-temperature counterparts, resulting in fewer active adsorption sites for PS-MNPs removal. By increasing the biochar dosage, the total number of available adsorption sites increases proportionally, enabling greater contaminant capture.

Moreover, higher biochar loading can enhance physical entrapment and aggregation effects. In suspension, PS-MNPs can interact with multiple biochar particles, and a denser biochar matrix improves the likelihood of layer trapping smaller particles. This is especially important for submicron-sized PS-MNPs (< 0.5 μm), where individual interactions with CCB350 may be weak due to limited van der Waals or electrostatic forces. A higher concentration of biochar increases the frequency of particle–bichar interactions, thereby improving overall removal efficiency. Additionally, increased biochar loading helps mitigate saturation effects, which are more pronounced at high PS-MNP concentrations. At lower dosages, adsorption sites on CCB350 can become saturated more rapidly, reducing efficiency. By maintaining a higher ratio of adsorption sites to contaminant particles, greater biochar loadings prevent early saturation and sustain high removal rates even in concentrated suspensions. These findings highlight that although CCB350 has a lower intrinsic adsorption capacity compared to CCB550 and CCB700, its performance can be strategically enhanced through increased biochar loading. This insight is particularly valuable for practical applications, where optimizing dosage may offer a cost-effective strategy to improve filtration efficiency when using lower-temperature biochars.

The adsorption mechanism of biochar was investigated through a combination of measurements on the biochar samples after adsorbing PS-MNPs. Biochar removes contaminants through complementary pathways, including layer trapping on biochar surfaces and pore-filling within the porous structure, with additional contribution from electrostatic interactions between charged biochar surfaces and contaminants (Fig. 9). SEM analysis further confirmed that MNPs were retained through layer trapping on biochar surfaces and pore-filling within internal pore structures, providing direct evidence for these structural retention pathways. The presence of PS-MNPs with an average size of 0.95 μm (Fig. 5a) and 2.1 μm (Fig. 5b) PS-MNPs firmly attached to the biochar layers suggests that the tightly packed microstructure facilitates physical entrapment, particularly for larger-sized particles. This mechanism enhances the effectiveness of biochar in retaining contaminants by preventing their passage through the filtration system (Schnee et al. 2016).

The porous structure of biochar was another means for MNP adsorption. SEM images (Fig. 9c) showed that the porous structure of biochar was partially or completely filled with MNPs, demonstrating that the pores provided internal sites for contaminant retention, which was confirmed by previous studies (Kaur et al. 2025). Additionally, evidence of compromised pore structures suggests that the biochar's porous framework actively participated in the adsorption process and underwent structural changes during PS-MNP uptake. BET analysis (Table 4) further underscores the importance of pore-based adsorption, revealing a significant reduction in total pore volume across all three biochar samples following the PS-MNPs treatments. In summary, PS-MNPs not only adhered to the biochar surface but also infiltrated and occupied internal pore spaces. The observed loss in pore volume highlights the critical role of porous architecture in determining biochar's adsorption capacity. Differences in pore volume reduction among the samples suggest that characteristics such as pore size distribution and structural integrity significantly influence adsorption performance. Notably, CCB550 and CCB700—both with higher initial pore volumes—retained more PS-MNPs than CCB350, implying that biochars with larger and more accessible pore networks offer enhanced adsorption potential. However, SEM imaging also revealed signs of structural degradation in some samples, indicating that excessive pore filling may compromise material stability and potentially impact long-term filtration efficiency. These findings emphasize the pivotal role of pore structure in contaminant removal and suggest that optimizing biochar porosity, such as through tailored pyrolysis conditions enhances adsorption performance, supporting its application in environmental filtration systems. Taken together, these results suggest that structural pathways play a dominant role in MNP retention. Particulate contaminants are primarily captured through layer trapping on surfaces and pore-filling within internal structures.

In addition to structural retention, electrostatic attraction also contributes significantly to the overall adsorption of MNPs by biochar. SEM analysis (Fig. 9d) revealed that MNPs adhered to the outer surface of biochar structures, suggesting an additional mechanism of interaction. Given that polystyrene typically carries a negative charge in neutral conditions, its behavior in this study indicates

a shift in surface charge due to the acidic suspension used for PS-MNP preparation. Under these conditions, the PS-MNPs acquired a positive surface charge, while biochar maintained its intrinsically negative zeta potential before adsorption. This charge contrast likely drove electrostatic attraction (which was also reported previously), leading to enhanced adsorption efficiency[65]. The zeta potential measurements before and after adsorption (Table 5) also supported this mechanism. Across all biochar samples, the zeta potential became less negative after PS-MNP treatment, indicating a partial neutralization of surface charges. This shift suggests that electrostatic interactions between negatively charged biochar and positively charged PS-MNPs played a crucial role in adhesion. The reduction in negative charge confirms that a portion of the biochar's active sites were occupied by positively charged contaminants, reinforcing the significance of electrostatic attraction in the adsorption process (Liu et al. 2022).

To further investigate the influence of solution chemistry, adsorption experiments were performed at different pH values (Table 6). Across all corn biochars, removal efficiency was highest under acidic conditions (pH 5.0), moderate at near-neutral pH (7.4), and lowest under alkaline conditions (pH 9.0). This pH dependence can be explained by changes in surface charge properties: under acidic conditions, protonation of functional groups reduces electrostatic repulsion and facilitates adhesion of PS-MNPs to biochar surfaces. In contrast, at alkaline pH, both PS-MNPs and biochars carry increased negative charges, leading to stronger electrostatic repulsion and reduced adsorption efficiency. These results provide direct functional evidence that electrostatics strongly influence MNP adsorption by biochar, consistent with previous findings for particulates–biochar interactions in aquatic systems (Siipola et al. 2020; Ahmad et al. 2014; Luyima et al. 2022).

In sum, these results suggest that structural pathways play a dominant role in MNP retention, with particulate contaminants primarily captured through layer trapping on surfaces and pore-filling within internal structures. Electrostatic attraction further enhances these processes, as PS-MNPs (under acidic suspension) adhere to negatively charged biochar surfaces. This integrated perspective reconciles the contributions of structural retention and surface chemistry in biochar-based filtration, and highlights the dual mechanism by which biochar achieves effective MNP removal.

4.4 Perspectives on safe and rational design of biochar for water treatment

In addition to adsorption efficiency, practical deployment requires assurance of environmental safety and filter reusability. Our 24-h leaching tests confirmed that none of the 16 EPA priority PAHs were detectable in filtrates, indicating negligible risk of secondary contamination during short-term aqueous filtration. Regeneration tests (Table 7) further demonstrated that corn cob biochars could be thermally re-pyrolyzed and reused for at least three cycles with only modest efficiency losses. For example, CCB350/2.5 remained statistically unchanged between Cycle 0 (40.93 ± 1.44%) and Cycle 1 (40.96 ± 1.22%) but declined significantly to 38.63 ± 1.16% and 33.68 ± 1.03% in Cycles 2 and 3, respectively. CCB550 showed a similar trend, remaining stable through Cycle 1 (46.48 ± 1.33% to 45.72 ± 1.17%) before decreasing to 43.19 ± 1.28% and 40.88 ± 1.15%. In contrast, CCB700 exhibited superior regeneration stability, with no significant differences across Cycles 0–2 (61.43 ± 2.29% to 58.72 ± 1.39%) and only a modest decline in Cycle 3 (55.41 ± 1.04%). These results provide direct evidence that the tested biochars are both environmentally safe and regenerable, supporting their feasibility for sustainable water treatment.

Building on these validated findings, future studies should broaden the design framework to optimize biochar for long-term and large-scale use. Kinetics remain an essential consideration, as they determine residence time and overall treatment capacity under continuous operation. In our flow-through funnel setup, the empty-bed contact time (EBCT) was approximately 1 min, yet the tested biochars still achieved the reported removal efficiencies. This rapid uptake suggests that surface interactions—such as electrostatic attraction and complexation for ammonia, and hydrophobic or π–π interactions for MNPs—dominate under short-contact conditions, while intraparticle diffusion may play a role over longer timescales. Time-resolved adsorption studies will therefore be valuable to quantify uptake rates and equilibrium times, providing design criteria for scaled filtration systems. In addition, advanced spectroscopic and computational tools—including FTIR, XPS, nano-SIMS, density functional theory (DFT), and molecular dynamics (MD)—offer opportunities to uncover adsorption energetics and predict optimal surface chemistries. Integrating such approaches with life-cycle and risk assessment frameworks can help ensure that new biochars deliver not only high removal efficiency but also durability and environmental safety across diverse treatment conditions.

Looking forward, advancing the safe and rational design of biochar requires more comprehensive characterization to connect structure with function. While this study focused on SEM, BET surface area, elemental composition, and zeta potential, future work should incorporate advanced spectroscopic and computational

approaches. Techniques such as FTIR, XPS, and nano-SIMS can provide detailed insights into surface functional groups and contaminant distributions, while density functional theory (DFT) and molecular dynamics (MD) simulations can reveal adsorption energetics and predict optimal surface chemistries. By integrating these tools with life-cycle and risk assessment frameworks, future studies can bridge fundamental science with applied engineering, ensuring that biochar not only performs efficiently but also remains environmentally safe and scalable for real-world water treatment. Advancing this line of research will require balancing adsorption efficiency with environmental safeguards, ensuring that biochars deliver high performance without introducing unintended risks. With such integrative approaches, biochar can progress from a promising laboratory material toward a reliable, scalable, and sustainable technology for water purification.

Biochar's demonstrated safety and reusability, together with its tunable physicochemical properties, position it as more than a laboratory adsorbent. With appropriate engineering, it can serve as a scalable platform technology that transforms agricultural residues into high-value materials for water purification. By integrating low-cost production with environmental safety and multi-cycle performance, biochar-based filters can be envisioned for use in decentralized and industrial treatment systems. Beyond water quality improvement, such applications contribute to waste valorization, carbon management, and circular economy objectives, highlighting biochar's potential to bridge environmental remediation with sustainable resource use at the global scale.

5 Conclusion

This study demonstrated that biochars derived from agricultural residues can effectively remove both ammonia and polystyrene micro/nanoplastics (PS-MNPs) from aqueous solutions, with performance strongly influenced by feedstock type and pyrolysis temperature. In comparative screening, woody feedstocks such as bamboo and walnut generated biochars with higher surface area and pore volume, while corn cob biochars provided balanced performance that warranted more detailed evaluation. Subsequent in-depth tests therefore focused on corn cob biochars prepared at different pyrolysis temperatures. Among these, CCB700 exhibited the highest ammonia adsorption capacity, maintaining removal rates of ~ 60% at 10 ppm, whereas CCB550 and CCB350 showed lower efficiencies under the same conditions. For MNP removal, the higher-temperature corn cob biochars (CCB550 and CCB700) achieved robust and consistent efficiencies (~ 90%) across particle sizes (0.1–2.1 μm), while CCB350 displayed selective removal favoring larger particles. Mechanistic analyses confirmed that contaminants were retained via complementary pathways, including surface trapping, pore filling, and electrostatic or hydrophobic interactions.

Beyond adsorption efficiency, this study validated two critical aspects of practical application. PAH leaching tests confirmed that none of the 16 EPA priority PAHs were detectable in filtrates, ensuring negligible risk of secondary contamination. Regeneration experiments further showed that corn cob biochars could be thermally re-pyrolyzed and reused for at least three cycles, with CCB700 retaining > 55% removal efficiency in Cycle 3. Together, these results establish that engineered biochars can function as effective, safe, and reusable materials, underscoring their potential as sustainable and scalable solutions for water purification. If deployed strategically, biochar not only addresses water quality challenges but also contributes to waste valorization, carbon management, and sustainable resource use.

Supplementary Information

The online version contains supplementary material available at https://doi.org/10.1007/s42773-025-00554-z.

Supplementary material 1

Acknowledgements
This work was supported by the Natural Resources Conservation Service, US Department of Agriculture, through the grant program Partnership for Climate-Smart Commodities, grant number: NR243A750004G028.

Author contributions
Ruogu Tang: Data curation, Formal Analysis, Investigation, Methodology, Software, Visualization, Writing-original draft; Siyu Qiu: Data curation, Formal Analysis, Investigation, Software, Visualization, Writing-original draft; Changqing Wu: Conceptualization, Funding acquisition, Methodology, Resources, Supervision, Writing-review & editing; Juzhong Tan: Conceptualization, Formal Analysis, Funding acquisition, Investigation, Methodology, Project administration, Resources, Supervision, Validation, Visualization, Writing-review & editing. All authors read and approved the final manuscript.

Funding
Natural Resources Conservation Service, NR243A750004G028, Juzhong Tan.

Data availability
The datasets used or analyzed during the current study are available from the corresponding author upon reasonable request. More information can be found here: https://www.springer.com/journal/44246/submission-guidelines#Instructions%20for%20Authors_Research%20Data%20Policy%20and%20Data%20Availability%20Statements

Declarations

Competing interests
The authors declare no competing interests.

Received: 19 June 2025 Revised: 1 December 2025 Accepted: 5 December 2025
Published online: 26 December 2025

References

Abbas Z, Ali S, Rizwan M et al (2018) A critical review of mechanisms involved in the adsorption of organic and inorganic contaminants through biochar. Arab J Geosci 11:448. https://doi.org/10.1007/s12517-018-3790-1

Ahmad M, Rajapaksha AU, Lim JE et al (2014) Biochar as a sorbent for contaminant management in soil and water: a review. Chemosphere 99:19–33. https://doi.org/10.1016/j.chemosphere.2013.10.071

Ahmed MB, Zhou JL, Ngo HH, Guo W, Chen M (2016) Progress in the preparation and application of modified biochar for improved contaminant removal from water and wastewater. Bioresour Technol 214:836–851. https://doi.org/10.1016/j.biortech.2016.05.057

Ambaye TG, Vaccari M, van Hullebusch ED et al (2021) Mechanisms and adsorption capacities of biochar for the removal of organic and inorganic pollutants from industrial wastewater. Int J Environ Sci Technol 18:3273–3294. https://doi.org/10.1007/s13762-020-03060-w

Amin AEEAZ (2018) Phosphorus dynamics and corn growth under applications of corn stalks biochar in a clay soil. Arab J Geosci 11:379. https://doi.org/10.1007/s12517-018-3719-8

Anand U, Dey S, Bontempi E et al (2023) Biotechnological methods to remove microplastics: a review. Environ Chem Lett 21:1787–1810. https://doi.org/10.1007/s10311-022-01552-4

Arbabi A, Gholami M, Farzadkia M et al (2023) Microplastics removal technologies from aqueous environments: a systematic review. J Environ Health Sci Engineer 21:463–473. https://doi.org/10.1007/s40201-023-00872-z

Babuji P, Thirumalaisamy S, Duraisamy K, Periyasamy G (2023) Human health risks due to exposure to water pollution: a review. Water 15:2532. https://doi.org/10.3390/w15142532

Boyce JM (2023) Quaternary ammonium disinfectants and antiseptics: tolerance, resistance and potential impact on antibiotic resistance. Antimicrob Resist Infect Control 12:32. https://doi.org/10.1186/s13756-023-01241-z

Bushra B, Remya N (2024a) Biochar from pyrolysis of rice husk biomass—characteristics, modification and environmental application. Biomass Convers Biorefin 14:5759–5770. https://doi.org/10.1007/s13399-020-01092-3

Bushra B, Remya N (2024b) Biochar from pyrolysis of rice husk biomass—characteristics, modification and environmental application. Biomass Conv Biorefin 14:5759–5770. https://doi.org/10.1007/s13399-020-01092-3

Buss W, Hilber I, Graham C et al (2022) Composition of PAHs in biochar and implications for biochar production. ACS Sustain Chem Eng 10(20):6755–6765. https://doi.org/10.1021/acssuschemeng.2c00952

Cai Y, Jiang W, Liu D et al (2023) Adsorption of sulfanilamides using biochar derived from *Suaeda salsa*: adsorption kinetics, isotherm, thermodynamics, and mechanism. Environ Sci Pollut Res 30:70528–70540. https://doi.org/10.1007/s11356-023-27228-2

Chen P (2024) Unlocking policy effects: water resources management plans and urban water pollution. J Environ Manag 365:121642. https://doi.org/10.1016/j.jenvman.2024.121642

Chen B, Zhou D, Zhu L (2008) Transitional adsorption and partition of nonpolar and polar aromatic contaminants by biochars of pine needles with different pyrolytic temperatures. Environ Sci Technol 42(14):5137–5143. https://doi.org/10.1021/es8002684

Chen W, Meng J, Han X et al (2019) Past, present, and future of biochar. Biochar 1:75–87. https://doi.org/10.1007/s42773-019-00008-3

Chen S, Zhong M, Wang H et al (2023) Study on adsorption of Cu^{2+}, Pb^{2+}, Cd^{2+}, and Zn^{2+} by the $KMnO_4$ modified biochar derived from walnut shell. Int J Environ Sci Technol Tehran 20:1551–1568. https://doi.org/10.1007/s13762-022-04002-4

Cosgove W, Loucks D (2015) Water management: current and future challenges and research directions. Water Resour Res 51:4823–4839. https://doi.org/10.1002/2014WR016869

Crini G, Lichtfouse E (2019) Advantages and disadvantages of techniques used for wastewater treatment. Environ Chem Lett 17:145–155. https://doi.org/10.1007/s10311-018-0785-9

Dey TK, Uddin ME (2021) Jamal m detection and removal of microplastics in wastewater: evolution and impact. Environ Sci Pollut Res 28:16925–16947. https://doi.org/10.1007/s11356-021-12943-5

Dias SLP, Neto CL, Ferreira VG et al (2025) Exploring the thermal degradation of pine nut shells: a study on biochar production and its efficacy in cationic dye adsorption from water. Biomass Conv Biorefin 15:5975–5995. https://doi.org/10.1007/s13399-024-05470-z

Fan Q, Sun J, Chu L et al (2018) Effects of chemical oxidation on surface oxygen-containing functional groups and adsorption behavior of biochar. Chemosphere 207:33–40. https://doi.org/10.1016/j.chemosphere.2018.05.044

Farghali M, Chen Z, Osman AI et al (2024) Strategies for ammonia recovery from wastewater: a review. Environ Chem Lett 22:2699–2751. https://doi.org/10.1007/s10311-024-01768-6

Fawzy S, Osman AI, Yang H et al (2021) Industrial biochar systems for atmospheric carbon removal: a review. Environ Chem Lett 19:3023–3055. https://doi.org/10.1007/s10311-021-01210-1

Gai X, Wang H, Liu J, Zhai L, Liu S, Ren T, Liu H (2014) Effects of feedstock and pyrolysis temperature on biochar absorption of ammonium and nitrate. PLoS ONE 9:e113888. https://doi.org/10.1371/journal.pone.0113888

Gao W, He W, Zhang J et al (2023) Effects of biochar-based materials on nickel adsorption and bioavailability in soil. Sci Rep 13:5880. https://doi.org/10.1038/s41598-023-32502-x

Ghodszad L, Reyhanitabar A, Oustan S (2021) Biochar effects on phosphorus sorption-desorption kinetics in soils with dissimilar acidity. Arab J Geosci 14:366. https://doi.org/10.1007/s12517-021-06629-y

Goswami L, Kushwaha A, Kafle SR, Kim B (2022) Surface modification of biochar for dye removal from wastewater. Catalysts 12(8):817. https://doi.org/10.3390/catal12080817

Haque A, Holsen TM, Baki ABM (2024) Distribution and risk assessment of microplastic pollution in a rural river system near a wastewater treatment plant, hydro-dam, and river confluence. Sci Rep 14:6006. https://doi.org/10.1038/s41598-024-56730-x

Joardar JC, Mondal B, Sikder S (2020) Comparative study of poultry litter and poultry litter biochar application in the soil for plant growth. SN Appl Sci 2:1770. https://doi.org/10.1007/s42452-020-03596-z

Kalsoom AA, Khan S, Ali N, Khan MA (2024) Enhanced ultrasonic adsorption of pesticides onto the optimized surface area of activated carbon and biochar: adsorption isotherm, kinetics, and thermodynamics. Biomass Conv Bioref. https://doi.org/10.1007/s13399-023-04170-4

Kaur K, Saleem M, Kaur H (2025) Biochar and biopolymer based nanomaterials for microplastic remediation: a sustainable approach for environment. Top Catal. https://doi.org/10.1007/s11244-025-02185-x

Kesari KK, Soni R, Jamal QMS et al (2021) Wastewater treatment and reuse: a review of its applications and health implications. Water Air Soil Pollut 232:208. https://doi.org/10.1007/s11270-021-05154-8

Kumar A, Bhattacharya T, Shaikh WA et al (2022) Biochar modification methods for augmenting sorption of contaminants. Curr Pollution Rep 8:519–555. https://doi.org/10.1007/s40726-022-00238-3

Kumar T, Ansari SA, Sawarkar R et al (2025) Bamboo biochar: a multifunctional material for environmental sustainability. Biomass Conv Bioref. https://doi.org/10.1007/s13399-025-06608-3

Li K, Du L, Qin C et al (2024) Microplastic pollution as an environmental risk exacerbating the greenhouse effect and climate change: a review. Carbon Res 3:9. https://doi.org/10.1007/s44246-023-00097-7

Liu Y, Ma J, Gao J et al (2022) Stability and interaction of biochar and iron mineral nanoparticles: effect of pH, ionic strength, and dissolved organic matter. Biochar 4:47. https://doi.org/10.1007/s42773-022-00172-z

Liu Z, Liu H, Zhang Y et al (2023) Efficient phosphate recycling by adsorption on alkaline sludge biochar. Environ Chem Lett 21:21–30. https://doi.org/10.1007/s10311-022-01527-5

Lu L, Yu W, Wang Y et al (2020) Application of biochar-based materials in environmental remediation: from multi-level structures to specific devices. Biochar 2:1–31. https://doi.org/10.1007/s42773-020-00041-7

Luo D, Wang L, Nan H et al (2023) Phosphorus adsorption by functionalized biochar: a review. Environ Chem Lett 21:497–524. https://doi.org/10.1007/s10311-022-01519-5

Luyima D, Egyir M, Lee JH et al (2022) A review of the potentiality of biochar technology to abate emissions of particulate matter originating from agriculture. Int J Environ Sci Technol 19:3411–3428. https://doi.org/10.1007/s13762-021-03267-5

Lyiola AO, Akinrinade AJ, Ajayi FO (2022) Effects of Water Pollution on Biodiversity Along the Coastal Regions. In: Chibueze Izah S (ed) Biodiversity in Africa: Potentials, Threats and Conservation Sustainable Development and Biodiversity. Springer, Singapore

Mahdi Z, Yu QJ, El Hanandeh A (2018) Removal of lead(II) from aqueous solution using date seed-derived biochar: batch and column studies. Appl Water Sci 8:181. https://doi.org/10.1007/s13201-018-0829-0

Mousavi M, Mehrzad J, Najafi MF et al (2022) Nitrate and ammonia: two key nitrogen sources for biomass and phycocyanin production by *Arthrospira*

(*Spirulina*) *platensis*. J Appl Phycol 34:2271–2281. https://doi.org/10.1007/s10811-021-02664-0
Müller YK, Wernicke T, Pittroff M et al (2020) Microplastic analysis-are we measuring the same? Results on the first global comparative study for microplastic analysis in a water sample. Anal Bioanal Chem 412:555–560. https://doi.org/10.1007/s00216-019-02311-1
Nair RR, Mondal MM, Weichgrebe D (2022) Biochar from co-pyrolysis of urban organic wastes—investigation of carbon sink potential using ATR-FTIR and TGA. Biomass Conv Biorefin 12:4729–4743. https://doi.org/10.1007/s13399-020-01000-9
Panwar NL, Pawar A (2022) Influence of activation conditions on the physicochemical properties of activated biochar: a review. Biomass Conv Biorefin 12:925–947. https://doi.org/10.1007/s13399-020-00870-3
Patel N, Srivastav AL, Patel A et al (2022) Nitrate contamination in water resources, human health risks and its remediation through adsorption: a focused review. Environ Sci Pollut Res Int 29:69137–69152. https://doi.org/10.1007/s11356-022-22377-2
Patra BR, Mukherjee A, Nanda S et al (2021) Biochar production, activation and adsorptive applications: a review. Environ Chem Lett 19:2237–2259. https://doi.org/10.1007/s10311-020-01165-9
Poerio T, Piacentini E, Mazzei R (2019) Membrane processes for microplastic removal. Molecules 24(22):4148. https://doi.org/10.3390/molecules24224148
Qiu S, Yuan M, Li M et al (2023) Phosphate adsorption on LDHs-biochar composite: double-layer model for quantifying the contribution of ion exchange and ligand exchange. Environ Sci Pollut Res 30:93986–93997. https://doi.org/10.1007/s11356-023-28958-z
Ravindiran G, Rajamanickam S, Janardhan G et al (2024) Production and modifications of biochar to engineered materials and its application for environmental sustainability: a review. Biochar 6:62. https://doi.org/10.1007/s42773-024-00350-1
Schnee LS, Knauth S, Hapca S et al (2016) Analysis of physical pore space characteristics of two pyrolytic biochars and potential as microhabitat. Plant Soil 408:357–368. https://doi.org/10.1007/s11104-016-2935-9
Sharma S, Bhardwaj A, Thakur M et al (2024) Understanding microplastic pollution of marine ecosystem: a review. Environ Sci Pollut Res 31:41402–41445. https://doi.org/10.1007/s11356-023-28314-1
Siipola V, Pflugmacher S, Romar H et al (2020) Low-cost biochar adsorbents for water purification including microplastics removal. Appl Sci 10(3):788. https://doi.org/10.3390/app10030788
Smith BC (1999) Infrared spectral interpretation: a systematic approach, 1st edn. CRC Press, USA
Subair A, Krishnamoorthy Lakshmi P, Chellappan S et al (2024) Removal of polystyrene microplastics using biochar-based continuous flow fixed-bed column. Environ Sci Pollut Res Int 31:13753–13765. https://doi.org/10.1007/s11356-024-32088-5
Thomas E, Borchard N, Sarmiento C et al (2020) Key factors determining biochar sorption capacity for metal contaminants: a literature synthesis. Biochar 2(2):151–163. https://doi.org/10.1007/s42773-020-00053-3
Tsai CH, Tsai WT, Liu SC et al (2018) Thermochemical characterization of biochar from cocoa pod husk prepared at low pyrolysis temperature. Biomass Conv Biorefin 8:237–243. https://doi.org/10.1007/s13399-017-0259-5
Weerasooriya RR, Liyanage LPK, Rathnappriya RHK et al (2021) Industrial water conservation by water footprint and sustainable development goals: a review. Environ Dev Sustain 23:12661–12709. https://doi.org/10.1007/s10668-020-01184-0
Xu H, Wang B, Zhao R et al (2022) Adsorption behavior and performance of ammonium onto sorghum straw biochar from water. Sci Rep 12:5358. https://doi.org/10.1038/s41598-022-08591-5
Zahra MB, Fayyaz B, Aftab ZEH et al (2022) Characterization and utilization of cow manure biochar as soil amendment for the management of northern corn leaf blight. J Soil Sci Plant Nutr 22:3348–3363. https://doi.org/10.1007/s42729-022-00891-z
Zhang Y, Zhang B, Yu J et al (2021) Functional biochar for efficient residue treatment of sulfonylurea herbicides by weak molecular interaction. Biochar 3:545–556. https://doi.org/10.1007/s42773-021-00111-4
Zhao M, Zou G, Li Y et al (2025) Biodegradable microplastics coupled with biochar enhance Cd chelation and reduce Cd accumulation in Chinese cabbage. Biochar 7(1):31. https://doi.org/10.1007/s42773-024-00418-y
Zhou R, Zhang M, Shao S (2022) Optimization of target biochar for the adsorption of target heavy metal ion. Sci Rep 12:13662. https://doi.org/10.1038/s41598-022-17901-w
Zhu Y, Qi B, Hao Y, Liu H, Sun G, Chen R, Song S (2021) Appropriate NH^{4+}/NO^{3-} ratio triggers plant growth and nutrient uptake of flowering Chinese cabbage by optimizing the pH value of nutrient solution. Front Plant Sci 12:656144. https://doi.org/10.3389/fpls.2021.656144